



Lu, D., Liang, J., Du, X., Wang, G. and Shire, T. (2019) A novel transversely isotropic strength criterion for soils based on a mobilized plane approach. *Geotechnique*, 69(3), pp. 234-250. (doi:[10.1680/jgeot.17.p.191](https://doi.org/10.1680/jgeot.17.p.191)).

This is the author's final accepted version.

There may be differences between this version and the published version. You are advised to consult the publisher's version if you wish to cite from it.

<http://eprints.gla.ac.uk/158694/>

Deposited on: 03 April 2018

Enlighten – Research publications by members of the University of Glasgow
<http://eprints.gla.ac.uk>

1 **A novel transversely isotropic strength criterion for soils**
2 **based on a mobilized plane approach**

3 Author 1

4 ● Dechun LU, Ph.D., Professor

5 ● Key Laboratory of Urban Security and Disaster Engineering of Ministry of Education, Beijing University of
6 Technology, Beijing 100124, China.

7 ● E-mail: dechun@bjut.edu.cn

8 Author 2

9 ● Jingyu LIANG (corresponding author), Ph.D. Candidate

10 ● Key Laboratory of Urban Security and Disaster Engineering of Ministry of Education, Beijing University of
11 Technology, Beijing, China.

12 ● E-mail: liangjingyuy@163.com

13 Author 3

14 ● Xiuli DU (major corresponding author), Ph.D., Professor

15 ● Key Laboratory of Urban Security and Disaster Engineering of Ministry of Education, Beijing University of
16 Technology, Beijing, China.

17 ● E-mail: duxiuli5@126.com

18 Author 4

19 ● Guosheng WANG, Ph.D. Candidate

20 ● Key Laboratory of Urban Security and Disaster Engineering of Ministry of Education, Beijing University of
21 Technology, Beijing, China.

22 ● E-mail: wangguosheng-12345@163.com

23 Author 5

24 ● Tom Shire, Ph.D., Lecturer

25 ● School of Engineering, University of Glasgow, Glasgow, UK.

26 ● E-mail: Thomas.shire@glasgow.ac.uk

27

28 ABSTRACT

29 The peak shear strength rules of transversely isotropic soils are stress state dependent and dependent on relative
30 orientation between bedding plane and principal stress. Accordingly, the shear strength of transversely isotropic
31 soils exhibits two primary characteristics: (i) the strength curve on the deviatoric plane is asymmetrical with
32 respect to three principal stress axes; (ii) the shear strength changes with the direction angle of the bedding plane
33 when the intermediate principal stress coefficient is a constant. In this paper, the mobilized plane is introduced and
34 used to reveal the failure mechanism of soils. By projecting the microstructure tensor of transversely isotropic
35 soils onto the normal of the mobilized plane, the directionality of the transversely isotropic soils is introduced into
36 the friction rules on the mobilized plane, and a transversely isotropic strength parameter is proposed. The
37 proposed strength parameter can extend isotropic strength criteria into transversely isotropic strength criteria. This
38 mobilized plane approach is used to establish a novel transversely isotropic nonlinear unified strength criterion
39 (TI-NUSC). The difficulty to establish a unified description of the asymmetrical strength curve and its evolution
40 with direction angle is overcome by the established criterion. Comparisons between available test results and the
41 TI-NUSC shows that the TI-NUSC can successfully describe these two primary peak strength characteristics.

42 KEYWORDS: Shear strength; Anisotropy; Fabric/structure of soils; Friction; Failure; Sands;

43 1 INTRODUCTION

44 Anisotropy is a significant property of soils and is intrinsically related to the microstructure of soils.
45 Anisotropic soils exhibit inherent and induced anisotropy (Casagrande & Carillo, 1944). Induced anisotropy is
46 attributed to plastic deformation associated with loading, while inherent anisotropy is typically treated as a fabric
47 property in the virgin state before any loadings occur. The simplest form of anisotropy is transverse isotropy,
48 which is a ubiquitous property of naturally deposited soils. The transverse isotropy has a remarkable influence on
49 the peak shear strength, which varies with the relative orientation between the loading and bedding plane. The
50 maximum variation of the bearing capacity for transversely isotropic soils in different loading directions is
51 approximately 35% (Oda *et al.*, 1978). Such a variation cannot be represented by the isotropic strength criteria.
52 The neglect of the transverse isotropy in engineering design is potentially hazardous. A proper description of the
53 strength variation rules for transversely isotropic soils has important implications for the analysis of slope stability
54 (Su & Liao, 1999) and the bearing capacity of shallow foundations (Fu & Dafalias, 2011) and embankments
55 (Zdravkovic *et al.*, 2002; Sun *et al.*, 2004), amongst other applications.

56 Laboratory tests have been conducted to study the strength characteristics of transversely isotropic soils.
57 These tests have included plane strain tests (Oda *et al.*, 1978; Tatsuoka *et al.*, 1990), true triaxial tests (Lam &
58 Tatsuoka, 1988; Kirkgard & Lade, 1993) and hollow cylinder tests (Nishimura *et al.*, 2007; Lade *et al.*, 2014;
59 Yang *et al.*, 2016). The experimental findings show that transversely isotropic soils exhibit two primary peak shear
60 strength characteristics: (i) The strength curve on the deviatoric plane is not symmetrical with respect to the three
61 principal stress axes when compared with the isotropic strength curve, meanwhile, the effects of the intermediate
62 principal stress coefficient $b = (\sigma_2 - \sigma_3) / (\sigma_1 - \sigma_3)$ on the strength parameter φ is no longer independent of stress
63 direction; (ii) the direction angle δ between the normal direction of the bedding plane and the vertical direction
64 greatly affects the peak shear strength and the strength parameter. Actually, the effects of δ and b are coupled and
65 the strength curve on the deviatoric plane evolves with δ .

66 Compared with the experimental study of peak strength characteristics, research into the corresponding
67 strength theory is poorly developed. In general, there are four methods to establish transversely isotropic strength
68 criteria. Firstly, mathematical method, such as the coordinate rotation method (Abelev & Lade, 2004) and the
69 method of modified Lode angle-based shape function (Mortara, 2010; Lü *et al.*, 2011), was proposed to describe
70 the asymmetry of the strength curve with respect to the three stress axes. However, these mathematical methods
71 are only applied to the coaxial condition, i.e., $\delta=0^\circ$. Secondly, the fabric tensor and the stress tensor can be
72 combined to establish a transversely isotropic strength criterion. The combined tensor of the fabric tensor and the
73 stress tensor was proposed (Tobita, 1988) and introduced into an isotropic strength criterion to describe the
74 strength characteristics of transversely isotropic soils (Yao *et al.*, 2017). Additionally, the joint invariant of the
75 stress tensor and fabric tensor has been defined (Li & Dafalias, 2002; Dafalias *et al.*, 2004) and used to develop
76 the strength criteria for transversely isotropic soils (Gao *et al.*, 2010; Gao & Zhao, 2012). Thirdly, the method of
77 projecting the microstructure tensor onto the generalized loading direction was proposed to establish transversely
78 isotropic strength criterion by defining an anisotropic parameter (Pietruszczak & Mroz, 2000; Pietruszczak &
79 Mroz, 2001). The anisotropic parameter could be ‘married’ to an isotropic criterion (Lade, 2007; Xiao *et al.*, 2012;
80 Kong *et al.*, 2013; Lü *et al.*, 2016). Nevertheless, the combination of the fabric/microstructure tensor and the
81 stress tensor can only characterize the monotonic decrease of the shear strength as δ increases but cannot describe
82 the non-monotonic variation rules of the shear strength. Thus, a high-order equation was suggested by
83 Pietruszczak & Guo (2013) and used to modify the Lade criterion (Rodriguez & Lade, 2013). It is a mathematical
84 approach, in which a least squares method based on polynomial regression was used to determine the parameters.
85 Consequently, not all parameters in the high-order equation have physical meanings. The fourth method is based
86 on a new view that the relative orientation between the mobilized plane and the fabric direction could be used to
87 reflect the non-monotonic variation rules of the shear strength (Liu & Indraratna, 2011; Yao & Kong, 2012;
88 Oboudi *et al.*, 2016; Chang & Bennett, 2017). However, the non-monotonic variation applies only to a constant b .

89 These methods can describe either of the two primary characteristics revealed by experiments, but they are not
90 good enough to describe both of them in a unified way.

91 This paper presents a novel strength criterion for transversely isotropic soils based on a mobilized plane
92 approach which can couple the effects of b and δ in a more physically meaningful way. The concept of the
93 mobilized plane is introduced to reveal the shear failure mechanism and the strength rules of transversely isotropic
94 soils. Firstly, a two dimensional (2D) strength parameter is proposed by projecting the 2D microstructure tensor
95 onto the direction of the mobilized plane to reveal effects of δ on strength rules. Then, a 3D transversely isotropic
96 strength parameter is proposed by a similar projection under the 3D stress condition. The TI-NUSC is established
97 by combining the 3D strength parameter and the NUSC. Comparisons between the established TI-NUSC and the
98 experimental data available indicates the reasonable predictive capability of the TI-NUSC on accounting the
99 effects of δ and b on peak shear strength rules of transversely isotropic soils.

100 2 SHEAR FAILURE MECHANISM OF TRANSVERSELY ISOTROPIC SOILS

101 Shear failure is assumed to occur when the ratio of shear stress (τ) to normal stress (σ) acting on a specific
102 plane reaches a critical value (Matsuoka & Nakai, 1974; Wood, 1990; Pietruszczak & Mroz, 2001; Liu &
103 Indraratna, 2011; Lu *et al.*, 2017; Ma *et al.*, 2017). The specific plane can be called the mobilized plane. For
104 isotropic materials, the mobilized plane depends only on the stress values when failure occurs, and it is
105 independent of the loading direction. The failure condition can be written as follows:

$$106 \quad \frac{\tau}{\sigma} = f(\Phi) \quad (1)$$

107 where Φ is a generalized material parameter. It can be the cohesive strength (c) and the internal friction angle (φ)
108 for soils, and only be φ for cohesionless soils.

109 The essences of the failure mechanism for soils are the direction of the mobilized plane and the critical value
110 that the shear-normal stress ratio can reach. For transversely isotropic materials, the determined method of the
111 mobilized plane is similar to that for isotropic materials. However, the direction of the mobilized plane and the

112 critical value that the shear-normal stress ratio can reach are all related not only to the stress values but also to the
 113 relative orientation between loading direction and bedding plane. The failure condition can be expressed as
 114 follows:

$$115 \quad \frac{\tau}{\sigma} = f(\Phi, \Theta) \quad (2)$$

116 where Θ is a generalized direction angle. As shown in Fig. 1, three components of Θ , i.e., δ , ω and θ , are direction
 117 angles of \mathbf{D} in the $Oxyz$ principal stress space, and two of them are independent due to the identical equation
 118 $\cos^2\delta + \cos^2\omega + \cos^2\theta = 1$.

119 Experimental works under the condition that δ or θ changes with $\omega=90^\circ$ have been conducted to study peak
 120 shear strength rules of transversely isotropic soils (Lam & Tatsuoka, 1988; Lade *et al.*, 2014; Yang *et al.*, 2016).
 121 But failure criteria to fully describe the experimental findings have not been developed. How to reveal and
 122 describe these experimental strength rules by the friction rule on the mobilized plane is a difficult and important
 123 task.

124 2.1 Microstructure tensor for transversely isotropic soils

125 The direction of the mobilized plane and the critical value that the shear-normal stress ratio can reach are
 126 closely related to the fabric of soils, which can be measured by a microstructure or fabric tensor \mathbf{A} (Tobita, 1988;
 127 Pietruszczak & Mroz, 2000) and quantified by the orientations of contacts, particles or voids (Yang *et al.*, 2008;
 128 Shire *et al.*, 2013). The eigenvalues of \mathbf{A} are expressed as a_1 , a_2 and a_3 . For transversely isotropic soils, $a_2=a_3$.
 129 Thus, tensor \mathbf{A} is represented as follows:

$$130 \quad \mathbf{A} = \begin{bmatrix} a_1 & 0 & 0 \\ 0 & a_3 & 0 \\ 0 & 0 & a_3 \end{bmatrix} = \eta_0 \left(\begin{bmatrix} \Omega_1 & 0 & 0 \\ 0 & \Omega_3 & 0 \\ 0 & 0 & \Omega_3 \end{bmatrix} + \begin{bmatrix} 1 & 0 & 0 \\ 0 & 1 & 0 \\ 0 & 0 & 1 \end{bmatrix} \right) \quad (3)$$

131 where $\eta_0=(a_1+2a_3)/3$ is the average value of the eigenvalues of \mathbf{A} and reflects the average level of material
 132 properties in different directions. Ω_1 and Ω_3 are the eigenvalues of the deviatoric tensor, and $\Omega_1+2\Omega_3=0$. Ω_1 or Ω_3
 133 reflects the degree of anisotropy.

134 In the plane perpendicular to the bedding plane, the transverse isotropy can be described by the 2D
 135 microstructure tensor \mathbf{A}^{2D} , which is

$$136 \quad \mathbf{A}^{2D} = \begin{bmatrix} a_1 & 0 \\ 0 & a_3 \end{bmatrix} = \eta_0^{2D} \left(\begin{bmatrix} \Omega_1 & 0 \\ 0 & \Omega_3 \end{bmatrix} + \begin{bmatrix} 1 & 0 \\ 0 & 1 \end{bmatrix} \right) \quad (4)$$

137 where $\eta_0^{2D} = (a_1 + a_3)/2$ is the average of the eigenvalues of \mathbf{A}^{2D} , and $\Omega_1 + \Omega_3 = 0$.

138 2.2 Effect of the directionality of transversely isotropic soils on strength rules

139 For a 2D stress state, the relative orientation between the bedding plane and mobilized plane is shown in Fig.
 140 2. Fig. 2(a) and Fig. 2(b) are schematic diagrams of the physics and geometry, respectively. As shown in Fig. 2(b),
 141 the z - and y -axes are the stress direction axes in the Oyz stress space, and the normal vector of the bedding plane is
 142 \mathbf{D} , which is coaxial with the z -axis in the Oyz physical space. The vector \mathbf{D} in Oyz can be represented by a
 143 trigonometric function of the direction angle δ , i.e., $\mathbf{D} = (\cos\delta, \sin\delta)$. ζ is the angle between \mathbf{D} and the normal vector
 144 of the critical mobilized plane, and $\zeta = \min(\zeta_1, \zeta_2)$, where ζ_1 is the angle between \mathbf{D} and the normal vector of
 145 mobilized plane 1, and ζ_2 is the angle between \mathbf{D} and the normal vector of mobilized plane 2. The normal vector of
 146 the critical mobilized plane is denoted as \mathbf{N}^{2D} in Oyz and as \mathbf{N}^{3D} in Oyz . The failure condition on the mobilized
 147 plane for cohesionless soils can be expressed as follows:

$$148 \quad \frac{\tau_n}{\sigma_n} = \tan \varphi \quad (5)$$

149 where $\tau_n = (\sigma_1 - \sigma_3)\sqrt{\sigma_1\sigma_3}/(\sigma_1 + \sigma_3)$ and $\sigma_n = 2\sigma_1\sigma_3/(\sigma_1 + \sigma_3)$ are the shear and normal stress acting on AC ,
 150 respectively. The equivalent form of Eq. (5), i.e., $\sqrt{\sigma_1/\sigma_3} = \tan(45^\circ + \varphi/2)$, is used to determine the position of
 151 AC , as shown in Fig. 2(b), and $OA = \sqrt{\sigma_1}$, $OC = \sqrt{\sigma_3}$. Thus, the normal vector of AC
 152 is $\mathbf{N}^{2D} = \left(\sqrt{\sigma_3/(\sigma_1 + \sigma_3)}, \sqrt{\sigma_1/(\sigma_1 + \sigma_3)} \right)$ in Oyz and is $\mathbf{N}^{3D} = (n_1^{2D}, n_3^{2D}) = (\cos\zeta, \sin\zeta)$ in Oyz .

153 The 2D transversely isotropic strength parameter is proposed by projecting the 2D microstructure tensor onto
 154 the normal vector (\mathbf{N}^{3D}) of the critical mobilized plane, which is similar to the definition of the anisotropic
 155 parameter by Pietruszczak and Mroz (2000).

156
$$\eta^{2D} = \mathbf{N}^{2D} \mathbf{A}^{2D} (\mathbf{N}^{2D})^T = \eta_0^{2D} \left[1 + \Omega_1 (\mathcal{H}_p^{2D})^2 + \Omega_3 (\mathcal{H}_\delta^{2D})^2 \right] \quad (6)$$

157 This projection of the 2D microstructure tensor onto the normal vector of the critical mobilized plane is the
 158 reflection of the effect of the 2D microstructure on frictional characteristics. That is, η^{2D} can reflect the changing
 159 rules of internal friction angle by combining Eq. (5) and Eq. (6), i.e., $\eta^{2D} = \tan \varphi|_\delta$. Where $\varphi|_\delta$ is an extended
 160 version of φ which varies with δ .

161
$$\frac{\tau_n}{\sigma_n} = \tan \varphi|_\delta = \eta_0^{2D} \left[1 + \Omega_1 (\mathcal{H}_p^{2D})^2 + \Omega_3 (\mathcal{H}_\delta^{2D})^2 \right] \quad (7)$$

162 Further, substituting $\Omega_1 + \Omega_3 = 0$ and $(\mathcal{H}_p^{2D})^2 + (\mathcal{H}_\delta^{2D})^2 = 1$ into Eq. (7) yields

163
$$\tan \varphi|_\delta = \eta_0^{2D} \left\{ 1 + \Omega_3 \left[1 - 2(\mathcal{H}_p^{2D})^2 \right] \right\} \quad (8)$$

164 where \mathcal{H}_p^{2D} is the cosine of ζ , which can be calculated in terms of \mathbf{N}^{2D} and \mathbf{D} .

165
$$\mathcal{H}_p^{2D} = \frac{\mathbf{N}^{2D} \cdot \mathbf{D}}{|\mathbf{N}^{2D}| |\mathbf{D}|} = \cos \delta \sqrt{\frac{\sigma_3}{\sigma_1 + \sigma_3}} + \sin \delta \sqrt{\frac{\sigma_1}{\sigma_1 + \sigma_3}} \quad (9)$$

166 $\mathcal{H}_p^{2D} = \cos(45^\circ + \varphi/2 - \delta)$ is derived by combining $\sigma_1/\sigma_3 = (1 + \sin \varphi|_\delta)/(1 - \sin \varphi|_\delta)$ with Eq. (9), thus, $\zeta = 45^\circ + \varphi|_\delta/2 - \delta$ is
 167 obtained. By substituting Eq. (9) into Eq. (8), we obtain an expression which describes how $\varphi|_\delta$ changes with δ .

168
$$\tan \varphi|_\delta = \eta_0^{2D} \left\{ 1 + \Omega_3 \left[1 - 2 \left(\cos \delta \sqrt{\frac{\sigma_3}{\sigma_1 + \sigma_3}} + \sin \delta \sqrt{\frac{\sigma_1}{\sigma_1 + \sigma_3}} \right)^2 \right] \right\} \quad (10)$$

169 Two material parameters η_0^{2D} and Ω_3 can be collectively solved by two linear equations which correspond
 170 $\varphi|_\delta$ at two different δ values. Taking the case of transversely isotropic Toyoura sand (Oda *et al.*, 1978) as a
 171 demonstrative example here. The friction angles $\varphi|_{\delta=0^\circ} = 49.44^\circ$ and $\varphi|_{\delta=90^\circ} = 44.22^\circ$ were obtained from plane
 172 strain tests on vertical ($\delta=0^\circ$) and horizontal ($\delta=90^\circ$) samples as shown in Fig. 3 for $\sigma_3=196$ kPa.
 173 $(\sigma_1/\sigma_3)|_{\delta=0^\circ} = 7.324$ and $(\sigma_1/\sigma_3)|_{\delta=90^\circ} = 5.610$ Therefore, $\eta_0^{2D}=1.067$ and $\Omega_3=0.126$ can be solved from Eq.
 174 (10).

175 The variation of η^{2D} associated with angle ζ_1 can be obtained from Eq. (8). As shown in Fig. 4, η^{2D} for
 176 mobilized plane 1 increases monotonously as ζ_1 increases from 0° to 90° . But for mobilized plane 2, the η^{2D}
 177 increases first and then decreases. Soil will fail along the critical mobilized plane which is close to the bedding

178 plane (i.e. the plane of weakness). The critical mobilized plane is mobilized plane 1 when $0^\circ \leq \zeta_1 < 69.72^\circ$ and is
179 shown as the red solid line. The critical mobilized plane can be either of the two mobilized plane and $\zeta_2 = \zeta_1$, when
180 $\zeta_1 = 69.72^\circ$. After this, $\zeta_2 < \zeta_1$, and the critical mobilized plane becomes mobilized plane 2 when $69.72^\circ < \zeta_1 \leq 90^\circ$ and
181 is shown as the green solid line in Fig. 4. The closer the mobilized plane is to the bedding plane, the more easily
182 the soil fails.

183 A further understanding of the failure mechanism of transversely isotropic soils can be obtained by the
184 correspondence between Fig. 4 and Fig. 5 in terms of the relationship between ζ_1 and δ ($\zeta_1 = 45^\circ + \varphi|_{\delta/2 - \delta}$).
185 Correspondingly, the relationship between η^{2D} and δ can be calculated using Eq. (10), as shown in Fig. 5. When
186 $0^\circ < \delta < 90^\circ$, the critical mobilized plane is mobilized plane 1 and η^{2D} initially decreases and then increases slightly
187 with δ . $A_\delta - B_\delta - C_\delta$ in Fig. 5 corresponds to $A_\zeta - B_\zeta - C_\zeta$ in Fig. 4. When $-90^\circ < \delta < 0^\circ$, the critical mobilized plane will be
188 mobilized plane 2, and the corresponding relationship illustrated by the green solid line in Fig. 5 is opposite to that
189 of $0^\circ < \delta < 90^\circ$. The theoretical predictions ($\varphi|_{\delta = \arctan \eta^{2D}}$) can capture the experimental observed non-monotonic
190 variation of φ with the increase of δ for the transversely isotropic sand (Oda *et al.*, 1978; Matsuoka *et al.*, 1984;
191 Tatsuoka *et al.*, 1990) as shown in Fig. 6.

192 3 3D TRANSVERSELY ISOTROPIC STRENGTH PARAMETER

193 Based on the understanding of the failure mechanism, a comprehensive and unified 3D transversely isotropic
194 strength parameter can be proposed by introducing the concept of the mobilized plane into the anisotropic
195 parameter. For isotropic soils under a 3D stress state, the position of the mobilized plane in the stress space is
196 closely related to the stress values only. The loading direction does not affect the shear strength characteristics,
197 and the φ - b relationship is constant. For transversely isotropic soils, soils themselves possess directionality. The
198 direction of the mobilized plane is affected by stress values and loading direction. The relative orientation between
199 the bedding plane and the mobilized plane will affect the peak shear strength characteristics (Liu & Indraratna,
200 2011; Yao & Kong, 2012) and needs to be analysed.

201 3.1 Relative orientation between the bedding plane and mobilized plane

202 The arbitrary relative orientation between the bedding plane and the mobilized plane can be described using
 203 two angles (Lam & Tatsuoka, 1988; Mroz & Maciejewski, 2002; Lü *et al.*, 2016). However, for the condition that
 204 $\omega=90^\circ$, that is x and z in coincide as shown in Fig. 7, one angle δ or θ ($\delta+\theta=90^\circ$) is sufficient to describe the
 205 relative orientation. The physical coordinate system $Oxyz$ is introduced for describing the direction of the
 206 mobilized plane in physical space, where the z -axis is coaxial with the normal vector \mathbf{D} of the bedding plane.
 207 The direction angle of \mathbf{D} in $Oxyz$ is δ ; thus, $\mathbf{D}=(\cos\delta, 0, \sin\delta)$. The normal vector of the mobilized plane ABC is \mathbf{N}
 208 in $Oxyz$, and $\mathbf{N}=(n_x, n_y, n_z)$. The direction cosine n_i ($i=x, y, z$) with respect to the σ_i axis can be expressed as
 209 follows:

210
$$n_i = \sqrt{\frac{\sigma_x \sigma_y \sigma_z}{\sigma_i (\sigma_x \sigma_y + \sigma_y \sigma_z + \sigma_z \sigma_x)}} \quad (11)$$

211 The normal vector of the mobilized plane in $Oxyz$ is expressed as $\mathbf{N}=(n_x, n_y, n_z)$. As shown in Fig. 7,
 212 $n_z = \cos\zeta$ and ζ is the angle between \mathbf{D} and \mathbf{N} . Thus, $n_z = n_z \cos\delta + n_y \sin\delta$ and can be used to describe the
 213 relative orientation of \mathbf{D} and \mathbf{N} .

214 The relative orientation between the normal of the bedding plane and the normal of the mobilized plane is
 215 closely related to the stress distribution that acts on a transversely isotropic soil element. Due to the directionality
 216 of transversely isotropic soils, effects of stress distribution is not symmetrical about the three principal stress axes.
 217 We can partition the deviatoric plane into six stress distribution sectors as shown in Fig. 8. The stresses σ_1, σ_2 and
 218 σ_3 acted on a transversely isotropic soil element are distributed in different directions in each sector. The
 219 symmetry of stress distributions is actually associated with δ . The symmetry axis will be the z -axis when $\delta=0^\circ$, the
 220 x -axis when $\delta=45^\circ$ and the y -axis when $\delta=90^\circ$. Accordingly, strength characteristics possess the same symmetry
 221 with the stress distribution.

222 3.2 A new 3D transversely isotropic strength parameter

223 The method of projection (Pietruszczak & Mroz, 2000; Pietruszczak & Mroz, 2001) is extended to 3D to
 224 propose a 3D transversely isotropic strength parameter. The effect of the 3D microstructure on the frictional
 225 strength is taken into account by projecting the 3D microstructure tensor \mathbf{A} onto the normal vector \mathbf{N} of the
 226 mobilized plane. When combined with the transversely isotropic condition, a 3D strength parameter η can be
 227 obtained:

$$228 \quad \eta = \eta_0 \left[1 + \Omega_3 (1 - 3m_\rho^2) \right] \quad (12)$$

229 where η_0 reflects the average value of η , and Ω_3 reflects the degree of anisotropy. m_ρ is a function that used to
 230 reflect the change rules of η with the increase of δ . To reflect the strength characteristics of different axes related
 231 to δ when $\omega=90^\circ$, a more comprehensive function with the following two features is proposed: (i) it is
 232 independent of δ along the x -axis ($\sigma_z=\sigma_y$); (ii) the change rules under the condition that $\sigma_x=\sigma_y$ or $\sigma_x=\sigma_z$ are
 233 adjustable. The function that satisfies these two features is the key to develop a 3D transversely isotropic strength
 234 parameter.

235 The following interpolation function m_ρ is used in this paper for describing these two features

$$236 \quad m_\rho = \rho\psi m_I + (1 - \rho\psi) m_{II} \quad (13)$$

237 where ρ is the distribution coefficient that controls the variability of η as δ increases. ψ is a stress state dependent
 238 function and its expression is

$$239 \quad \psi = \frac{(\sigma_z - \sigma_y)^2}{(\sigma_z - \sigma_x)^2 + (\sigma_x - \sigma_y)^2 + (\sigma_y - \sigma_z)^2} \quad (14)$$

240 where $\psi=0$ when $\sigma_z=\sigma_y$, and Eq. (13) becomes $m_\rho = m_{II}$; $\psi=1/2$ when $\sigma_x=\sigma_y$ or $\sigma_x=\sigma_z$, and Eq. (13) becomes
 241 $m_\rho = 1/2 \rho m_I + (1 - 1/2 \rho) m_{II}$.

242 In Eq. (13), $m_I = \mathbf{N} \cdot \mathbf{N}$ is the direction cosine of \mathbf{N} , and its expression is $m_I = n_z \cos \delta + n_y \sin \delta$. m_{II} ensures
 243 that the strength parameter η along the x -axis ($\sigma_z=\sigma_y$) is independent of δ , specified by the relationship:

$$244 \quad m_{II} = n_z \cos^2 \delta + n_y \sin^2 \delta \quad (15)$$

245 By substituting Eqs. (14)-(15) together with $m_I = n_z \cos \delta + n_y \sin \delta$ into Eq. (13), a comprehensive expression
 246 of m_ρ that satisfies the two features mentioned above can be derived. Then, the expression of η is obtained from
 247 Eq. (12) as follows:

$$248 \quad \eta = \eta_0 + \eta_0 \Omega_3 \left\{ 1 - 3 \left[\rho \psi (n_z \cos \delta + n_y \sin \delta) + (1 - \rho \psi) (n_z \cos^2 \delta + n_y \sin^2 \delta) \right] \right\} \quad (16)$$

249 It can be used to reflect strength variation rules for different stress distribution. For the stress state of the
 250 x -axis ($\sigma_z = \sigma_y$), $\psi = 0$ and $n_z = n_y = \sigma_x / (2\sigma_x + \sigma_y)$, η describes the strength parameter variation rules of the x -axis, and is
 251 expressed as follows:

$$252 \quad \eta = \eta_0 \left[1 + \Omega_3 (1 - m_{II}) \right] = \eta_0 \left[1 + \Omega_3 (1 - 3n_z) \right] \quad (17)$$

253 Eq. (17) indicates that η is independent of δ when $\sigma_z = \sigma_y$. For the stress state of the z -axis ($\sigma_x = \sigma_y$) or y -axis ($\sigma_x = \sigma_z$),
 254 $\psi = 1/2$ is obtained from Eq. (14) and Eq. (12) becomes

$$255 \quad \eta = \eta_0 + \eta_0 \Omega_3 \left\{ 1 - 3 \left[\frac{1}{2} \rho (n_z \cos \delta + n_y \sin \delta) + \left(1 - \frac{1}{2} \rho \right) (n_z \cos^2 \delta + n_y \sin^2 \delta) \right]^2 \right\} \quad (18)$$

256 As shown in Fig. 9, the trend of η changes from monotonic for $\rho = 0$ (the dashed line) to non-monotonic for $\rho = 2$
 257 (the solid line) when $\sigma_x = \sigma_y$.

258 The 3D transversely isotropic strength parameter η possesses the two features mentioned above and makes it
 259 possible to describe the coupled effects of b and δ in a unified way. In the following section η is combined with an
 260 isotropic strength criterion to develop a transversely isotropic strength criterion.

261 4 TRANSVERSELY ISOTROPIC NONLINEAR UNIFIED STRENGTH CRITERION

262 The NUSC (Yao *et al.*, 2004; Lu, 2006; Du *et al.*, 2010; Wang *et al.*, 2018) is applicable to various isotropic
 263 geomaterials, including soil, concrete, and rock. The failure surface of the NUSC in principal stress space is
 264 continuous, smooth and convex as shown in Fig. 10. Strength curve on the deviatoric plane, which reflects the
 265 effect of b on the shear strength, can continuously change from the Drucker-Prager (D-P) strength circle (upper
 266 bound) to the Matsuoka-Nakai (M-N) strength curved triangle (lower bound). By using a power function, the

267 cohesion effect, friction effect and hydrostatic pressure effect can be characterized on the meridian plane.

268 Expression of the NUSC can be written as

$$269 \quad \frac{\bar{q}_\alpha}{\bar{p}} = \alpha \frac{3\sqrt{\bar{I}_1^2 - 3\bar{I}_2}}{\bar{I}_1} + (1-\alpha) \frac{6}{3\sqrt{(\bar{I}_1\bar{I}_2 - \bar{I}_3)/(\bar{I}_1\bar{I}_2 - 9\bar{I}_3)} - 1} = M_f \quad (19)$$

270 where \bar{q}_α is the equivalent shear strength, $\bar{p} = (\bar{\sigma}_1 + \bar{\sigma}_2 + \bar{\sigma}_3)/3$ is mean stress in the transitional stress space. α

271 is a material parameter that reflects the triaxial extension-compression strength ratio at the reference stress, and M_f

272 is the failure stress ratio at the reference stress. \bar{I}_1 , \bar{I}_2 and \bar{I}_3 are the first, second and third stress invariants in

273 the transitional stress space respectively, defined as

$$274 \quad \begin{cases} \bar{I}_1 = \bar{\sigma}_1 + \bar{\sigma}_2 + \bar{\sigma}_3 \\ \bar{I}_2 = \bar{\sigma}_1\bar{\sigma}_2 + \bar{\sigma}_2\bar{\sigma}_3 + \bar{\sigma}_3\bar{\sigma}_1 \\ \bar{I}_3 = \bar{\sigma}_1\bar{\sigma}_2\bar{\sigma}_3 \end{cases} \quad (20)$$

275 The stress tensor in the transitional stress space is expressed as

$$276 \quad \bar{\sigma}_{ij} = \sigma_{ij} + \left[p_r \left(\frac{p + \sigma_0}{p_r} \right)^n - p \right] \delta_{ij} \quad (21)$$

277 where $p = (\sigma_1 + \sigma_2 + \sigma_3)/3$ is the mean stress, p_r is the reference stress, σ_0 is the three-dimensional tensile

278 strength, n is the hydrostatic pressure effect index and δ_{ij} is the Kronecker symbol.

279 4.1 Nonlinear unified strength criterion for transversely isotropic soils

280 Due to the parameter independence and extensibility of the NUSC, the 3D strength parameter η can be easily

281 introduced into the NUSC. For cohesionless soils, $\sigma_0=0$ and $n=1$, the simplified form of the NUSC adopted in this

282 study can be expressed as

$$283 \quad \frac{q_\alpha}{p} = \alpha \frac{3\sqrt{I_1^2 - 3I_2}}{I_1} + (1-\alpha) \frac{6}{3\sqrt{(I_1I_2 - I_3)/(I_1I_2 - 9I_3)} - 1} = M_f \quad (22)$$

284 where M_f degrades into the stress ratio in normal stress space when $\sigma_0=0$ and $n=1$. It is the reflection of the

285 frictional characteristics, which can be calculated by the internal friction angle φ_c under triaxial compressive

286 conditions, i.e., $M_f=6\sin\varphi_c/(3-\sin\varphi_c)$. I_1 , I_2 and I_3 are the first, second and third stress invariants in the normal

287 stress space respectively, defined as

$$288 \quad \begin{cases} I_1 = \sigma_1 + \sigma_2 + \sigma_3 \\ I_2 = \sigma_1\sigma_2 + \sigma_2\sigma_3 + \sigma_3\sigma_1 \\ I_3 = \sigma_1\sigma_2\sigma_3 \end{cases} \quad (23)$$

289 The frictional characteristics of transversely isotropic soils are strongly dependent on the loading direction
 290 (Imam *et al.*, 2002; Lade, 2008; Gao *et al.*, 2010). Thus, taking η as an extension of the failure stress ratio M_f , the
 291 TI-NUSC can be expressed as follows:

$$292 \quad \frac{q_\alpha}{p} = \frac{1}{p} \left[\alpha \sqrt{I_1^2 - 3I_2} + (1 - \alpha) \frac{2I_1}{3\sqrt{(I_1I_2 - I_3)/(I_1I_2 - 9I_3)} - 1} \right] = \eta_0 \left[1 + \Omega_3 (1 - 3m_\rho^2) \right] \quad (24)$$

293 Fig. 11 provides a graphical comparison of the NUSC and TI-NUSC when $\delta=0^\circ$ at the same internal friction
 294 angle $\varphi_c|_{\delta=0^\circ}$. It clearly shows that the TI-NUSC strength surface is asymmetrical with respect to σ_x - and σ_y -axes.

295 4.2 Coupled effects of b and δ on strength rules

296 The effects of b on strength rules within each of the six stress distribution sectors introduced in Fig. 8 are the
 297 same for isotropic soils and can be well described by the NUSC. But for transversely isotropic soils, effects of b
 298 are no longer symmetrical about three principal stress axes at the same time. Strength rules are closely related to
 299 the stress distributions in the six sectors when δ is constant. The coupled effects of b and δ make transversely
 300 isotropic soils exhibit the two primary peak shear strength characteristics described in the introduction.

301 4.2.1 Effects of b on strength rules when $\delta=0^\circ$

302 As shown in Fig. 12, three stress distribution sectors are sufficient due to the symmetry with respect to the
 303 σ_z -axis when $\delta=0^\circ$. In this case, Eq. (13) becomes

$$304 \quad m_\rho = n_z = \sqrt{\frac{\sigma_x\sigma_y}{\sigma_x\sigma_y + \sigma_y\sigma_z + \sigma_z\sigma_x}} \quad (25)$$

305 The stresses (σ_1 , σ_2 and σ_3) are distributed in these three sectors as shown in Fig. 12. Thus, the specific
 306 expression of m_ρ can be obtained from Eq. (25) in terms of $R=\sigma_1/\sigma_3$ and b in these sectors as follows:

307 In sector I ($\sigma_x=\sigma_2$, $\sigma_y=\sigma_3$ and $\sigma_z=\sigma_1$):

308
$$m_\rho = \sqrt{\frac{(bR - b + 1)}{R(bR - b + 1) + (bR - b + 1) + R}} \quad (26)$$

309 In sector II ($\sigma_x = \sigma_1$, $\sigma_y = \sigma_3$ and $\sigma_z = \sigma_2$):

310
$$m_\rho = \sqrt{\frac{R}{R(bR - b + 1) + (bR - b + 1) + R}} \quad (27)$$

311 In sector III ($\sigma_x = \sigma_1$, $\sigma_y = \sigma_2$ and $\sigma_z = \sigma_3$):

312
$$m_\rho = \sqrt{\frac{R(bR - b + 1)}{R(bR - b + 1) + (bR - b + 1) + R}} \quad (28)$$

313 η_0 and Ω_3 in Eq. (24) can be obtained from internal friction angles measured under triaxial compression
 314 perpendicular and along the bedding plane ($\varphi_c|_{\delta=0^\circ}$ and $\varphi_c|_{\delta=90^\circ}$). For conventional triaxial compression condition
 315 (i.e., $b=0$), Eq. (24) can be simplified in terms of the principal stress ratio $R_c (= (1 + \sin\varphi_c)/(1 - \sin\varphi_c))$

316
$$\frac{q_\alpha}{p} = \eta_c = \frac{3(R_c - 1)}{R_c + 2} = \eta_0 \left[1 + \Omega_3 (1 - 3m_\rho^2) \right] \quad (29)$$

317 where $\eta_c|_{\delta=0^\circ}$ and $\eta_c|_{\delta=90^\circ}$ can be obtained from the left side of Eq. (29), and $m_\rho|_{\delta=0^\circ}$ and $m_\rho|_{\delta=90^\circ}$ can be
 318 obtained from Eq. (26) and Eq. (28), respectively. These are substituted into Eq. (29) and a binary system of linear
 319 equations is thus obtained:

320
$$\begin{cases} \eta_c|_{\delta=0^\circ} = \eta_0 \left[1 + \Omega_3 (1 - 3m_\rho^2|_{\delta=0^\circ}) \right] \\ \eta_c|_{\delta=90^\circ} = \eta_0 \left[1 + \Omega_3 (1 - 3m_\rho^2|_{\delta=90^\circ}) \right] \end{cases} \quad (30)$$

321 η_0 and Ω_3 are then collectively solved by Eq. (30).

322 On the same deviatoric plane, $p=200$ kPa and $\alpha=1/3$ is taken as a special case for demonstration. For a fixed
 323 value of $\varphi_c|_{\delta=0^\circ} = 35^\circ$ and values of $\varphi_c|_{\delta=90^\circ}$ between 30° and 40° , the solved values of η_0 and Ω_3 are listed in
 324 [Table 1](#).

325 As shown in [Fig. 13](#), the fixed value of $\varphi_c|_{\delta=0^\circ} = 35^\circ$ makes each strength curve on the deviatoric plane pass
 326 through the same point, and the TI-NUSC curves are symmetrical with respect to σ_z only. The NUSC curve is
 327 shown by a black solid line when $\varphi_c|_{\delta=90^\circ} = 35^\circ$. As $\varphi_c|_{\delta=90^\circ}$ increases from 35° to 40° , η_0 increases, and Ω_3

328 decreases from 0. The size of the corresponding TI-NUSC curves increase, which means that the shear strength
329 along the bedding plane is higher than that along the normal of the bedding plane. As $\varphi_c|_{\delta=90^\circ}$ decreases from 35°
330 to 30° , η_0 decreases, and Ω_3 increases from 0. The size of the corresponding TI-NUSC curves decrease, as the
331 bedding plane is the plane of weakness.

332 As indicated by the solid dots in Fig. 13, the maximum shear strength dots of the TI-NUSC are close to but
333 not directly on the σ_x - and σ_y -axes. The maximum shear strength dots are in sector II when $\Omega_3 > 0$, and the
334 maximum shear strength dots are in sector III when $\Omega_3 < 0$. The maximum shear strength move further away from
335 the axes as the absolute value of Ω_3 increases.

336 Corresponding to Fig. 13, Fig. 14 shows the φ - b curves for different values of $\varphi_c|_{\delta=90^\circ}$. In sector I, σ_1 is
337 perpendicular to the bedding plane. The φ - b curves for different $\varphi_c|_{\delta=90^\circ}$ are almost the same. Thus, the effect of
338 anisotropy on φ can be ignored in this sector. In sector II, σ_2 is perpendicular to the bedding plane, and the effect
339 of anisotropy increases significantly as b decreases from 1 to 0. In sector III, σ_3 is perpendicular to the bedding
340 plane. There are a series of approximately parallel φ - b curves for different $\varphi_c|_{\delta=90^\circ}$. The φ - b curves and the
341 corresponding stress distribution in sectors IV, V and VI are symmetrical to these in sectors III, II and I,
342 respectively. The NUSC can be used to approximately describe the strength behaviour when the stress distribution
343 is consistent with that in sector I. In sector III, the approximately parallel φ - b curves could also be estimated by
344 multiplying φ_c in the NUSC by a scaling factor, particularly when the degree of anisotropy is small. However, the
345 transverse isotropy must be considered by η when the stress distribution is consistent with that in sector II, that is,
346 the isotropic strength criterion is incapable of describing behaviour under these conditions.

347 The effects of η_0 or Ω_3 can also be obtained, in a similar way to previous analysis. For a given value of
348 $\Omega_3=0.186$, the effect of η_0 on the strength curve on the deviatoric plane is shown in Fig. 15. The strength curves
349 vary from a quasi-circle to a curved triangle on the same deviatoric plane as η_0 increases. For a given value of
350 $\eta_0=1.267$, the effect of Ω_3 on the strength curve is shown in Fig. 16. The strength curves seem to be pulled up as

351 Ω_3 increases.

352 The value of α , which reflects the triaxial extension-compression strength ratio, is constant for a given
353 geomaterial. As α changes from 0 to 1, the corresponding TI-NUSC curves are shown in Fig. 17 for
354 $\varphi_c|_{\delta=0^\circ} = 35^\circ$ and $\varphi_c|_{\delta=90^\circ} = 30^\circ$. There are a series of continuous, smooth and convex strength curves, in which
355 the lower bound ($\alpha=0$) and upper bound ($\alpha=1$) are derived from the M-N criterion and D-P criterion, respectively.
356 The maximum shear strength dots for $\alpha=0$ are in sector II rather than on the σ_x - and σ_y -axes. As α increases, the
357 dots in sector II move further away from the σ_x - and σ_y -axes. For $\alpha=1$, the maximum shear strength dots return to
358 the $-\sigma_x$ - and $-\sigma_y$ -axes.

359 4.2.2 Effects of δ on strength rules

360 Four parameters $\eta_0=1.267$, $\Omega_3=0.186$, $\alpha=1/3$ and $\rho=1.200$ are taken as a case study to analyse the effect of δ
361 on the strength rules of transversely isotropic soils. The strength curves on the deviatoric plane of $p=200$ kPa with
362 the different δ values are predicted in Fig. 18. The strength curves of δ ($=0^\circ, 22.5^\circ, 45^\circ$) shown in Fig. 18(a) and
363 those of $90^\circ-\delta$ ($=90^\circ, 67.5^\circ, 45^\circ$) shown in Fig. 18(b) are symmetrical about the σ_x -axis. The maximum shear
364 strength dots of the strength curves close to the principal stress axes also change with δ , as shown by solid dots in
365 Fig. 18. The corresponding φ - b curves are shown in Fig. 19. The φ - b curves in sectors I-VI of Fig. 19(a) are the
366 same with that in sectors IV-III-II-I-VI-V of Fig. 19(b), which also corresponds to the symmetry of strength
367 curves. As δ increases from 0° to 90° , the variations of φ in sectors II, I and VI are predicted as shown in Fig. 20.
368 The variations of φ as δ increases in sectors III, IV and V are inversely symmetric with those in sectors II, I and VI,
369 respectively.

370 4.2.3 Coupled effects of b and δ on strength rules

371 The strength curves shown in Fig. 18 can be extended into a strength surface shown in Fig. 21, which shows
372 that the strength curve on the deviatoric plane evolves with δ . The non-monotonic variation of shear strength
373 under the triaxial compression as δ increases is illustrated by this strength surface. Correspondingly, the coupled

374 effect of b and δ on the strength parameter φ can be described by the φ - δ - b surface as shown in Fig. 22, which is
 375 the combination of Fig. 19 and Fig. 20. It is shown that the φ - b curve evolves with δ and the φ - δ curve changes
 376 with b in each of six sectors. These two variation rules shown in Fig. 22 are associated with the material direction
 377 and stress condition, respectively.

378 4.3 Determined methods of material parameters

379 There are four material parameters, i.e., η_0 , Ω_3 , α and ρ , with clear physical meaning in the established
 380 TI-NUSC. These material parameters can be determined by at least four specific types of test results, as shown in
 381 Fig. 23.

382 4.3.1 Determination of η_0 and Ω_3

383 $\varphi_c|_{\delta=0^\circ}$ and $\varphi_c|_{\delta=90^\circ}$ are used to solve η_0 and Ω_3 from Eq. (30). $\varphi_c|_{\delta=0^\circ}$ and $\varphi_c|_{\delta=90^\circ}$ are the internal friction
 384 angles obtained under conventional triaxial compression from samples with $\delta=0^\circ$ and $\delta=90^\circ$, respectively, as
 385 shown in Fig. 23(a) and (b).

386 4.3.2 Determination of α

387 The method for calculating α for isotropic soils (Yao *et al.*, 2004; Lu, 2006; Du *et al.*, 2010) can be extended
 388 for transversely isotropic soils with a constant direction angle δ as follows:

$$389 \quad \alpha = \frac{\left(\frac{q_e}{q_c} \right) - \left(\frac{q_e}{q_c} \right)_{MN}}{\left(\frac{q_e}{q_c} \right)_{DP} - \left(\frac{q_e}{q_c} \right)_{MN}} \Bigg|_{\delta} \quad (31)$$

390 Under the condition that $\delta=0^\circ$ and $q_c = (q_c)_{MN} = (q_c)_{DP}$, Eq. (31) can be transformed into Eq. (32).

$$391 \quad \alpha = \frac{\eta_e|_{\delta=0^\circ} - \eta_{MN}|_{\delta=0^\circ}}{\eta_{DP}|_{\delta=0^\circ} - \eta_{MN}|_{\delta=0^\circ}} \quad (32)$$

392 In Eq. (32), $\eta_{DP}|_{\delta=0^\circ} = 3(R_e|_{\delta=0^\circ} - 1)/(2R_e|_{\delta=0^\circ} + 1)$, $\eta_{MN}|_{\delta=0^\circ} = 3(R_e|_{\delta=0^\circ} - 1)/(R_e|_{\delta=0^\circ} + 2)$ and

393 $\eta_e|_{\delta=0^\circ} = \eta_0[1 + \Omega_3(R_e|_{\delta=0^\circ} - 1)/(R_e|_{\delta=0^\circ} + 2)]$, where $R_e|_{\delta=0^\circ} = (1 + \sin \varphi_e|_{\delta=0^\circ})/(1 - \sin \varphi_e|_{\delta=0^\circ})$. $\varphi_e|_{\delta=0^\circ}$ is the friction

394 angle obtained from the sample with $\delta=0^\circ$ under conventional triaxial extension, as shown in Fig. 23(c).

395 4.3.3 Determination of ρ

396 ρ is required to capture the variation of shear strength as δ increases from 0° to 90° . Samples with $0^\circ < \delta < 90^\circ$
397 as shown in Fig. 23(d) are tested under triaxial compression. The obtained internal friction angle $\varphi_c|_\delta$ is used to
398 calculate ρ , and the expression can be transformed from Eq. (24).

$$399 \quad \rho = \frac{2}{(m_I - m_{II})} \left(\sqrt{\frac{\eta_0 + \eta_0 \Omega_3 - \eta_c|_\delta}{3\eta_0 \Omega_3}} - m_{II} \right) \quad (33)$$

400 In Eq. (33), $\eta_c|_\delta = (q_\alpha/p)_c|_\delta = 3(R_c|_\delta - 1)/(R_c|_\delta + 2)$, where $R_c|_\delta = (1 + \sin \varphi_c|_\delta)/(1 - \sin \varphi_c|_\delta)$. m_I and m_{II} can
401 be obtained from Eq. (15) based on $R_c|_\delta$.

402 5 VERIFICATION

403 An experimental database has been compiled to study the coupled effects of δ and b on the peak shear
404 strength behaviour of transversely isotropic soils when $\omega=90^\circ$ and to verify the proposed criterion. The database
405 comprises Toyoura sand (Lam & Tatsuoka, 1988), Nevada sand (Lade *et al.*, 2014) and Leighton Buzzard sand
406 (Yang *et al.*, 2016). Material parameters are determined based on the determined method of this paper and listed in
407 Table 2.

408 5.1 Toyoura sand

409 Air-pluviated Toyoura sand was tested by Lam & Tatsuoka (1988) to study the effects of b and initial
410 anisotropic fabric on the peak shear strength. Drained tests in triaxial compression ($b=0$), plane strain ($b \approx 0.3$) and
411 triaxial extension ($b=1$) were performed when $\omega=90^\circ$ and $\delta=0^\circ, 30^\circ, 60^\circ$ and 90° . The shear strength data for
412 $\sigma_3=98$ kPa are summarized and found to be strongly influenced by b and δ . Five test results circled in Fig. 24 are
413 used to determine the material parameters listed in Table 2, where the two points labelled 4 are the same test
414 results displayed at different locations. Points 1 and 4 are used to determine η_0 and Ω_3 . Subsequently, α can be
415 obtained from point 5 by combining values of η_0 and Ω_3 . Four points, i.e., 1, 2, 3 and 4, are used to determine ρ .
416 The evolution of the TI-NUSC curves with δ for Toyoura sand is shown in Fig. 24. The test data and predicted

417 curve on the deviatoric plane are compared in Fig. 25 for the case of $\delta=0^\circ$. The isotropic NUSC strength curve
418 with the same $\varphi_c|_{\delta=0^\circ}$ is also shown. The availability of the TI-NUSC is verified by comparing the test data with
419 the predicted strength surface and curve in Fig. 24 and Fig. 25. The comparison shows that the peak shear strength
420 variation rules of Toyoura sand can be well captured by the proposed strength criterion.

421 5.2 Nevada sand

422 A total of 44 drained torsion shear tests on fine Nevada sand were performed by Lade *et al.* (2014) with an
423 initial effective confining stress of 100 kPa and with 25 combinations of constant b and δ . The open circles shown
424 in Fig. 26 are the original data from Figs. 8-12 in the original paper (Lade *et al.*, 2014). If there is more than one
425 point around the target δ - and b -values, the average of the internal friction angles is taken for comparison, as
426 indicated by the solid squares in Fig. 26. The 25 test points obtained are shown by the red cube in Fig. 27. Four
427 test results are sufficient to determine the material parameters. However, additional test data are needed because of
428 the discrete nature of the test results. Ten test points that are circled and numbered as 1-10 in Fig. 27 are used to
429 determine the material parameters. Points 1 and 5 are used to determine η_0 and Ω_3 . After that, point 6 together
430 with 1 and point 10 together with 5 are used to determine α . The triaxial compression test points 1, 2, 3, 4 and 5
431 can be used to obtain $\rho|_{b=0}=1.08$ as listed in Table 2, and the triaxial extension test points 7, 8, and 9 together with
432 η_0 , Ω_3 and α can be used to determine $\rho|_{b=1}=2.224$. Thus, the average value $\rho=1.652$ can be obtained to capture the
433 variation of the internal friction angle with δ . Fig. 27 and Fig. 28 give a comprehensive comparison between the
434 test data and predicted curves. The effects of δ and b on φ of transversely isotropic Nevada sand shown in Fig. 27
435 can be well captured by the proposed criterion. The effects of δ and b on peak shear strength can be captured by
436 the evolution of the strength curve, as shown in Fig. 28. Fig. 29 shows a comparison between the test data and the
437 strength curves on the deviatoric plane predicted by the TI-NUSC and the isotropic NUSC. The overall
438 satisfactory performance of the TI-NUSC in predicting the strength rules for Nevada sand can be observed at each
439 δ value.

440 5.3 Leighton Buzzard sand

441 A series of hollow cylinder torsional shear tests were performed by Yang *et al.* (2016) on dense Leighton
442 Buzzard sand with various combinations of δ and b . The angle δ of the samples were 0° , 15° , 30° , 60° , 75° and
443 90° . The intermediate principal stress coefficient b was set as 0, 0.2, 0.5 and 1 with a constant mean effective
444 stress of $p=200$ kPa. The test results are shown by dots in Fig. 30-Fig. 32. Seven points circled and numbered as
445 1-7 in Fig. 30 are used to determine the material parameters. Points 1 and 6 are used to determine η_0 and Ω_3 .
446 Points 2, 3, 4 and 5 together with η_0 and Ω_3 can determine ρ . α is determined by points 1 and 7. The determined
447 material parameters are listed in Table 2. The comparison between the test data and the φ - δ - b surface predicted by
448 the TI-NUSC is shown in Fig. 30. The effects of δ and b on peak shear strength are captured by the evolution of
449 the TI-NUSC strength curve as shown in Fig. 31. The variation rules that the strength parameter φ and the peak
450 shear strength decrease initially decreases and then increases when b is constant are well captured as shown in Fig.
451 30 and Fig. 31. The clearer comparisons between the test data and the strength curves predicted by the TI-NUSC
452 and the NUSC with $\varphi_c|_{\delta=0^\circ}=37.23^\circ$ on the deviatoric plane are shown in Fig. 32. The predicted surfaces and
453 curves can properly capture the coupled effects of b and δ in a unified way as shown by comparisons with
454 experimental data.

455 6 CONCLUSIONS

456 In this paper, the failure mechanism of soils was introduced and analysed for transversely isotropic soils. The
457 essences of the failure mechanism, i.e., the direction of the mobilized plane and the critical value that the
458 shear-normal stress ratio acting on that plane can reach are all affected by the microstructure of transversely
459 isotropic soils. Based on the understanding of the failure mechanism, the effects of the directionality of
460 transversely isotropic soils on shear strength rules were analysed. And further, a comprehensive and unified 3D
461 transversely isotropic strength parameter was proposed. The proposed strength parameter can reflect the variation
462 of the shear strength with the direction angle of the bedding plane. The TI-NUSC was then established by

463 combining the 3D transversely isotropic strength parameter with the NUSC. Two primary strength characteristics
464 that the asymmetry of the strength curve with respect to the three principal stress axes and variability of shear
465 strength with the bedding plane direction angle δ can thus be reflected in a unified way.

466 Four material parameters are included in the TI-NUSC. These material parameters have clear physical
467 meanings and can be easily determined by conventional triaxial tests. The established TI-NUSC was verified
468 favourably against available test data of transversely isotropic soils. Furthermore, the strength surface is
469 continuous, smooth and convex and could be used to construct elastoplastic constitutive models for transversely
470 isotropic soils. This mobilized plane approach for establishing transversely isotropic strength criteria could also be
471 suitable for developing strength criteria for other geomaterials, like concrete or rock.

472 ACKNOWLEDGEMENTS

473 This study was supported by the National Key Research and Development Program of China (Grant No.
474 2016YFC0701104), the National Natural Science Foundation of China (Grant Nos. 51522802, 51778026,
475 51421005, 51538001) and the National Natural Science Foundation of Beijing (8161001).

476

477 REFERENCES

- 478 Abelev, A. V., and Lade, P. V. (2004). Characterization of failure in cross-anisotropic soils. *Journal of Engineering*
479 *Mechanics, ASCE*. **130**, No. 5, 599-606.
- 480 Casagrande, A., and Carillo, N. (1944). Shear failure of anisotropic materials. *Boston Society of Civil Engineering*
481 *Journal*. **31**, No. 2, 74-87.
- 482 Chang, C. S., and Bennett, K. (2017). Micromechanical modeling for the deformation of sand with noncoaxiality
483 between the stress and material axes. *Journal of Engineering Mechanics*. **143**, No. 1, 1-15.
- 484 Dafalias, Y. F., Papadimitriou, A. G., and Li, X. S. (2004). Sand plasticity model accounting for inherent fabric
485 anisotropy. *Journal of Engineering Mechanics, ASCE*. **130**, No. 11, 1319-1333.
- 486 Du, X. L., Lu, D. C., Gong, Q. M., and Zhao, M. (2010). Nonlinear unified strength criterion for concrete under
487 three-dimensional stress states. *Journal of Engineering Mechanics, ASCE*. **136**, No. 1, 51-59.
- 488 Fu, P. C., and Dafalias, Y. F. (2011). Study of anisotropic shear strength of granular materials using DEM simulation.
489 *International Journal for Numerical and Analytical Methods in Geomechanics*. **35**, No. 10, 1098-1126.
- 490 Gao, Z. W., Zhao, J. D., and Yao, Y. P. (2010). A generalized anisotropic failure criterion for geomaterials. *International*
491 *Journal of Solids and Structures*. **47**, No. 22-23, 3166-3185.
- 492 Gao, Z. W., and Zhao, J. D. (2012). Efficient approach to characterize strength anisotropy in soils. *Journal of*
493 *Engineering Mechanics, ASCE*. **138**, No. 12, 1447-1456.
- 494 Imam, S. M. R., Chan, D. H., Robertson, P. K., Morgenstern, N. R., and Abelev, A. V. (2002). Effect of anisotropic

495 yielding on the flow liquefaction of loose sand. *Soils and Foundations*. **42**, No. 2, 33-44.

496 Kirkgard, M. M., and Lade, P. V. (1993). Anisotropic three-dimensional behavior of a normally consolidated clay.

497 *Canadian Geotechnical Journal*. **30**, No. 5, 848-858.

498 Kong, Y. X., Zhao, J. D., and Yao, Y. P. (2013). A failure criterion for cross-anisotropic soils considering microstructure.

499 *Acta Geotechnica*. **8**, No. 6, 665-673.

500 Lade, P. V. (2007). Modeling failure in cross-anisotropic frictional materials. *International Journal of Solids and*

501 *Structures*. **44**, No. 16, 5146-5162.

502 Lade, P. V. (2008). Failure criterion for cross-anisotropic soils. *Journal of Geotechnical and Geoenvironmental*

503 *Engineering, ASCE*. **134**, No. 1, 117-124.

504 Lade, P. V., Rodriguez, N. M., and Van Dyck, E. J. (2014). Effects of Principal Stress Directions on 3D Failure

505 Conditions in Cross-Anisotropic Sand. *Journal of Geotechnical and Geoenvironmental Engineering, ASCE*. **140**, No.

506 2, 1-12.

507 Lam, W., and Tatsuoka, F. (1988). Effects of initial anisotropic fabric and σ_2 on strength and deformation characteristics

508 of sand. *Soils and Foundations*. **28**, No. 1, 89-106.

509 Li, X. S., and Dafalias, Y. F. (2002). Constitutive Modeling of Inherently Anisotropic Sand Behavior. *Journal of*

510 *Geotechnical and Geoenvironmental Engineering*. **128**, No. 10, 868-880.

511 Liu, M. D., and Indraratna, B. N. (2011). General strength criterion for geomaterials including anisotropic effect.

512 *International Journal of Geomechanics, ASCE*. **11**, No. 3, 251-261.

513 Lu, D. C. (2006). *A constitutive model for soils considering complex stress paths based on the generalized nonlinear*

514 *strength theory*. PhD thesis, Beihang University, Beijing, China (in Chinese)

515 Lu, D. C., Ma, C., Du, X. L., Jin, L., and Gong, Q. M. (2017). Development of a new nonlinear unified strength theory

516 for geomaterials based on the characteristic stress concept. *International Journal of Geomechanics, ASCE*. **17**, No. 2,

517 04016058.

518 Lü, X. L., Huang, M. S., and Andrade, J. E. (2016). Strength criterion for cross-anisotropic sand under general stress

519 conditions. *Acta Geotechnica*. **11**, No. 6, 1339-1350.

520 Lü, X. L., Huang, M. S., and Qian, J. G. (2011). The onset of strain localization in cross-anisotropic soils under true

521 triaxial condition. *Soils and Foundations*. **51**, No. 4, 693-700.

522 Ma, C., Lu, D. C., Du, X. L., and Zhou, A. N. (2017). Developing a 3D elastoplastic constitutive model for soils: a new

523 approach based on characteristic stress. *Computers and Geotechnics*. **86**, 129-140.

524 Matsuoka, H., and Nakai, T. (1974). Stress-deformation and strength characteristics of soil under three different

525 principal stresses. *Proceedings of the Japan Society of Civil Engineers*. **232**, 59-70.

526 Matsuoka, H., Junichi, H., and Kiyoshi, H. (1984). Deformation and failure of anisotropic sand deposits. *Soil*

527 *Mechanics and Foundation Engineering*. **32**, No. 11, 31-36.

528 Mortara, G. (2010). A yield criterion for isotropic and cross-anisotropic cohesive-frictional materials. *International*

529 *Journal for Numerical and Analytical Methods in Geomechanics*. **34**, No. 10, 953-977.

530 Mroz, Z., and Maciejewski, J. (2002). Failure criteria of anisotropically damaged materials based on the critical plane

531 concept. *International Journal for Numerical and Analytical Methods in Geomechanics*. **26**, No. 4, 407-431.

532 Nishimura, S., Minh, N. A., and Jardine, R. J. (2007). Shear strength anisotropy of natural London Clay. *Géotechnique*.

533 **57**, No. 1, 49-62.

534 Oboudi, M., Pietruszczak, S., and Razaqpur, A. G. (2016). Description of inherent and induced anisotropy in granular

535 media with particles of high sphericity. *International Journal of Geomechanics, ASCE*. **16**, No. 4, 04016006.

536 Oda, M., Koishikawa, I., and Higuchi, T. (1978). Experimental study of anisotropic shear strength of sand by plane

537 strain test. *Soils and Foundations*. **18**, No. 1, 25-38.

538 Pietruszczak, S., and Guo, P. J. (2013). Description of deformation process in inherently anisotropic granular materials.

539 *International Journal for Numerical and Analytical Methods in Geomechanics*. **37**, No. 5, 478-490.

540 Pietruszczak, S., and Mroz, Z. (2000). Formulation of anisotropic failure criteria incorporating a microstructure tensor.

541 *Computers and Geotechnics*. **26**, No. 2, 105-112.

542 Pietruszczak, S., and Mroz, Z. (2001). On failure criteria for anisotropic cohesive-frictional materials. *International*
543 *Journal for Numerical and Analytical Methods in Geomechanics*. **25**, No. 5, 509-524.

544 Rodriguez, N. M., and Lade, P. V. (2013). Effects of principal stress directions and mean normal stress on failure
545 criterion for cross-anisotropic sand. *Journal of Engineering Mechanics, ASCE*. **139**, No. 11, 1592-1601.

546 Shire, T., O'Sullivan, C., Barreto, D., and Gaudray, G. (2013). Quantifying stress-induced anisotropy using inter-void
547 constrictions. *Géotechnique*. **63**, No. 1, 85-91.

548 Su, S. F., and Liao, H. J. (1999). Effect of strength anisotropy on undrained slope stability in clay. *Géotechnique*. **49**, No.
549 2, 215-230.

550 Sun, D. A., Matsuoka, H., Yao, Y. P., and Ishii, H. (2004). An anisotropic hardening elastoplastic model for clays and
551 sands and its application to FE analysis. *Computers and Geotechnics*. **31**, No. 1, 37-46.

552 Tatsuoka, F., Nakamura, S., Huang, C., and Tani, K. (1990). Strength anisotropy and shear band direction in plane strain
553 tests of sand. *Soils and Foundations*. **30**, No. 1, 35-54.

554 Tobita, Y. (1988). Yield condition of anisotropic granular materials. *Soils and Foundations*. **28**, No. 2, 113-126.

555 Wang, G. S., Lu, D. C., Du, X. L., and Zhou, X. (2018). Dynamic multiaxial strength criterion for concrete based on
556 strain rate – dependent strength parameters. *Journal of Engineering Mechanics*. **144**, No. 5, 4018018.

557 Wood, D. M. (1990). Soil behaviour and critical state soil mechanics. Cambridge University Press, Cambridge.

558 Xiao, Y., Liu, H. L., and Yang, G. (2012). Formulation of cross-anisotropic failure criterion for granular material.
559 *International Journal of Geomechanics*. **12**, No. 2, 182-188.

560 Yang, L. T., Li, X., Yu, H. S., and Wanatowski, D. (2016). A laboratory study of anisotropic geomaterials incorporating
561 recent micromechanical understanding. *Acta Geotechnica*. **11**, No. 5, 1111-1129.

562 Yang, Z. X., Li, X. S., and Yang, J. (2008). Quantifying and modelling fabric anisotropy of granular soils.
563 *Géotechnique*. **58**, No. 4, 237-248.

564 Yao, Y. P., Lu, D. C., Zhou, A. N., and Zou, B. (2004). Generalized non-linear strength theory and transformed stress
565 space. *Science in China Ser. E Engineering & Materials Science*. **47**, No. 6, 691-709.

566 Yao, Y. P., Tian, Y., and Gao, Z. W. (2017). Anisotropic UH model for soils based on a simple transformed stress method.
567 *International Journal for Numerical and Analytical Methods in Geomechanics*. **41**, No. 1, 54-78.

568 Yao, Y. P., and Kong, Y. X. (2012). Extended UH model: three-dimensional unified hardening model for anisotropic
569 clays. *Journal of Engineering Mechanics, ASCE*. **138**, No. 7, 853-866.

570 Zdravkovic, L., Potts, D. M., and Hight, D. W. (2002). The effect of strength anisotropy on the behaviour of
571 embankments on soft ground. *Géotechnique*. **52**, No. 6, 447-457.

NOTATION

\mathbf{A}^{2D}	2D microstructure tensor
\mathbf{A}	3D microstructure tensor
a_1, a_2, a_3	eigenvalues of the microstructure tensor
$\Omega_1, \Omega_2, \Omega_3$	eigenvalues of the deviatoric microstructure tensor
\mathbf{D}	normal vector of the bedding plane
d_1, d_2, d_3	direction cosines of the normal vector \mathbf{D}
δ, ω, θ	direction angle of the normal vector \mathbf{D} in the $Oxyz$ principal stress space
\mathbf{N}^{2D}	normal vector of the mobilized plane in the Oyz stress space
$\tilde{\mathbf{N}}^{2D}$	normal vector of the mobilized plane in the $O\tilde{y}\tilde{z}$ physical space
$\tilde{n}_1^{2D}, \tilde{n}_3^{2D}$	direction cosines of $\tilde{\mathbf{N}}^{2D}$ in the $O\tilde{y}\tilde{z}$ physical space
\mathbf{N}	normal vector of the mobilized plane in the $Oxyz$ stress space
n_x, n_y, n_z	direction cosines of \mathbf{N} in the $Oxyz$ stress space
$\tilde{\mathbf{N}}$	normal vector of the mobilized plane in the $O\tilde{x}\tilde{y}\tilde{z}$ physical space
$\tilde{n}_x, \tilde{n}_y, \tilde{n}_z$	direction cosines of $\tilde{\mathbf{N}}$ in the $O\tilde{x}\tilde{y}\tilde{z}$ physical space
ζ	angle between the bedding plane and mobilized plane
$\sigma_x, \sigma_y, \sigma_z$	principal stresses
I_1, I_2, I_3	first, second and third stress invariants
$\bar{I}_1, \bar{I}_2, \bar{I}_3$	first, second and third stress invariants in the in the transitional stress space
τ, σ	shear and normal stress acting on the mobilized plane
p	mean principal stress ($p=1/3(\sigma_1+\sigma_2+\sigma_3)$)
q	deviatoric stress ($q=1/\sqrt{2}\sqrt{(\sigma_1-\sigma_2)^2+(\sigma_2-\sigma_3)^2+(\sigma_3-\sigma_1)^2}$)

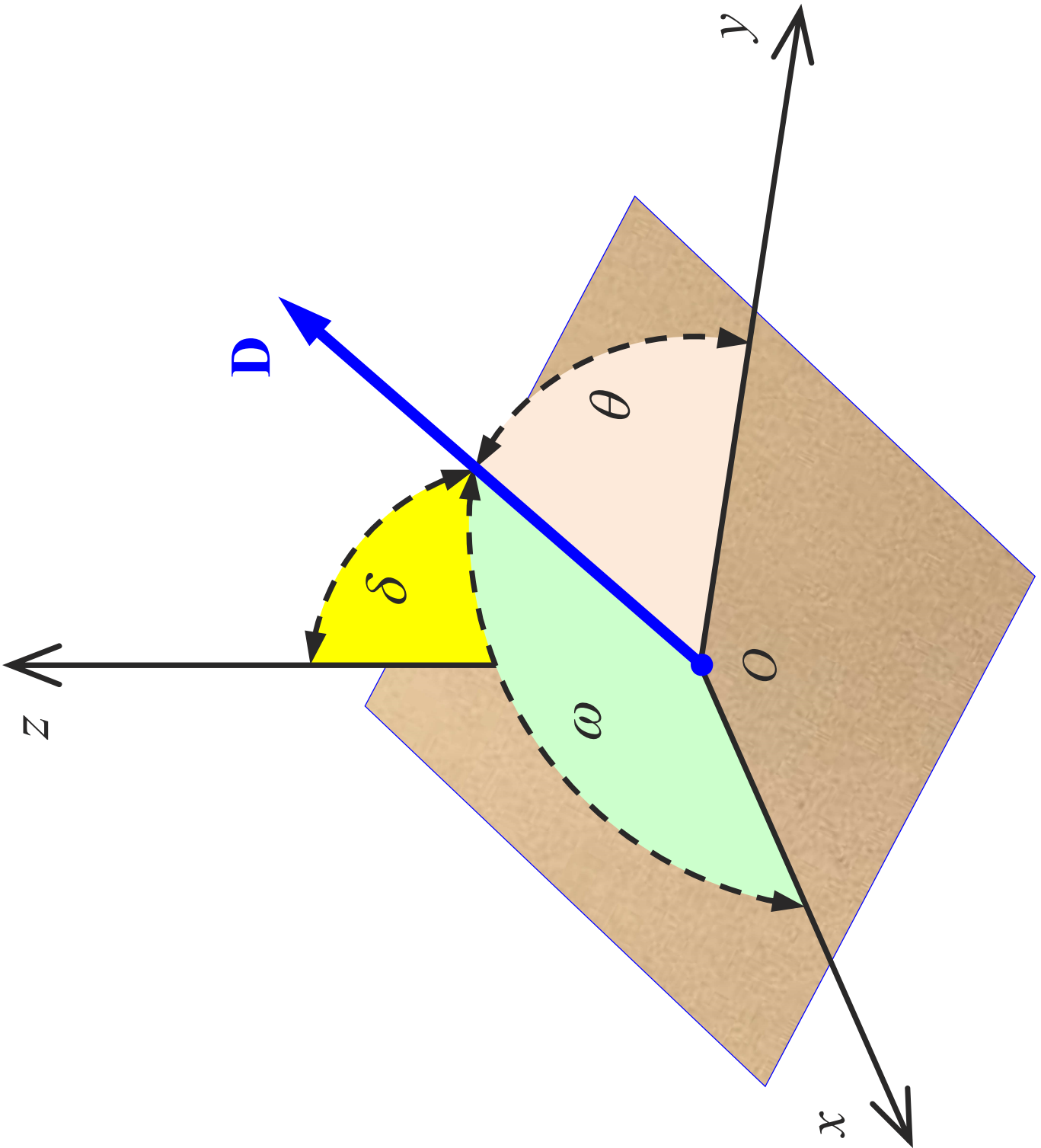
M_f	failure stress ratio
R	principal stress ratio ($R = \sigma_1 / \sigma_3$)
b	intermediate principal stress coefficient ($b = (\sigma_2 - \sigma_3) / (\sigma_1 - \sigma_3)$)
φ	internal friction angle
φ_c	internal friction angle under triaxial compressive conditions
φ_e	internal friction angle under triaxial extensive conditions
η^{2D}	2D transversely isotropic strength parameter
η_0^{2D}	average value of η^{2D}
η	3D transversely isotropic strength parameter
η_0	average value of a_1 , a_2 and a_3
η_c	stress ratio under triaxial compressive conditions
η_e	stress ratio under triaxial extensive conditions
α	triaxial extension–compression strength ratio
ρ	distribution coefficient
Φ	generalized material parameter
Θ	generalized direction angle

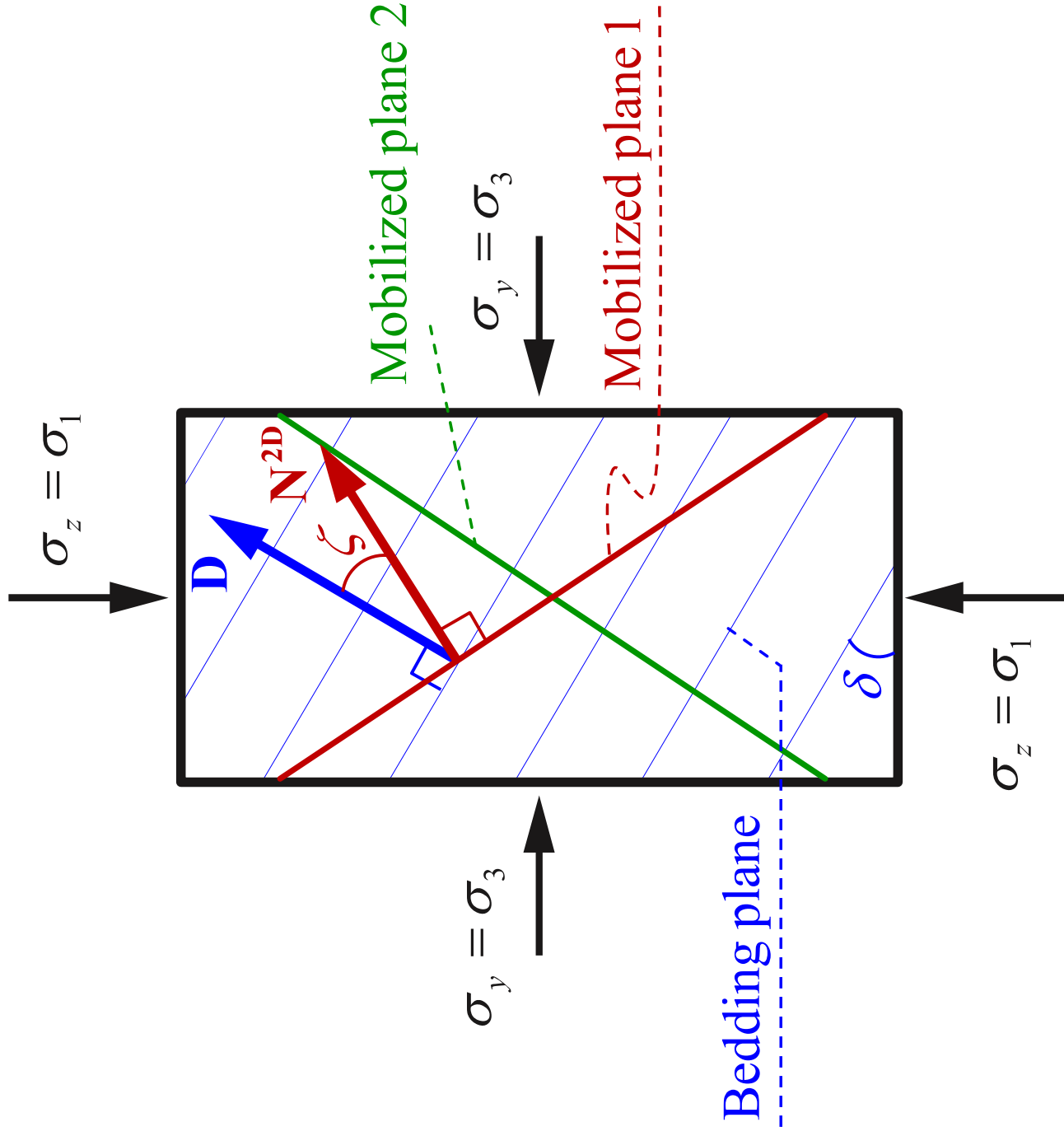
Table 1 Material parameter values for demonstration

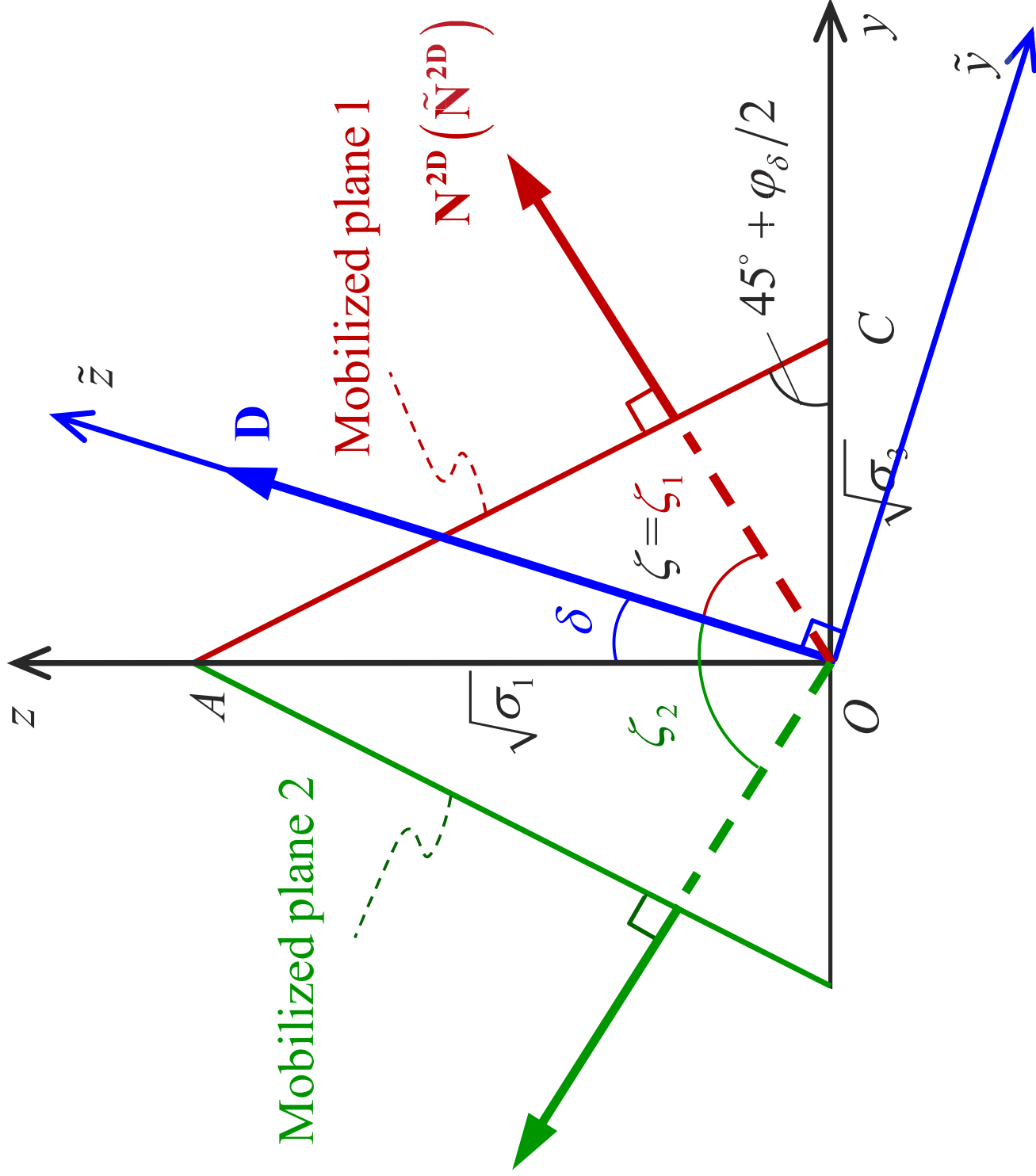
$\varphi_c _{\delta=0^\circ}$	$\varphi_c _{\delta=90^\circ}$	η_0	Ω_3
	40°	1.559	-0.140
	37.5°	1.490	-0.075
35°	35°	1.418	0
	32.5°	1.344	0.086
	30°	1.267	0.186

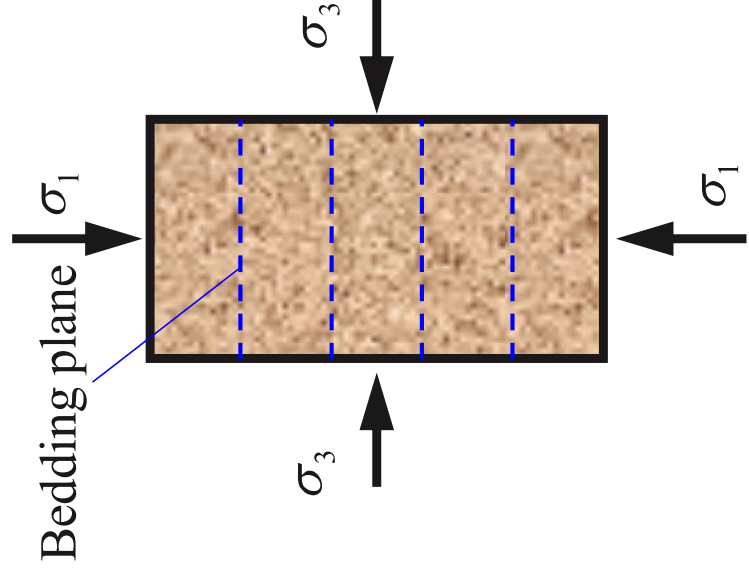
Table 2 Values of the material parameters for the TI-NUSC

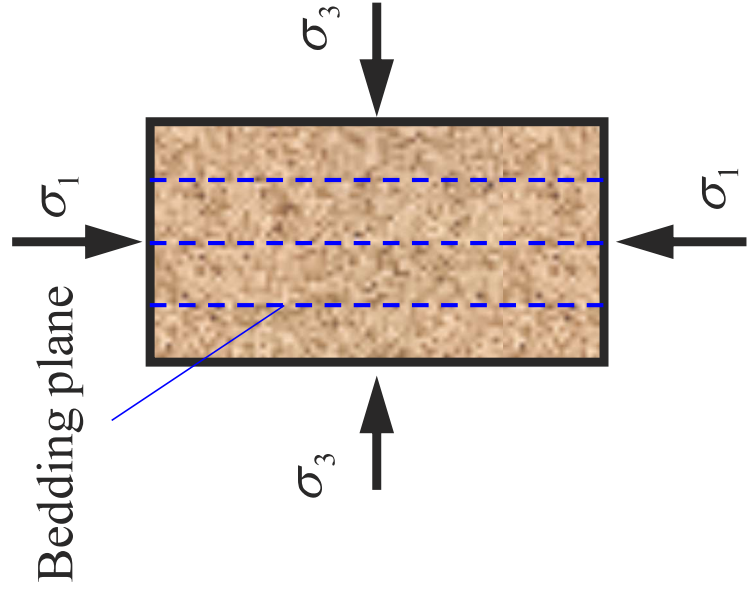
Soils	η_0	Ω_3	α	ρ
Toyoura sand (Lam & Tatsuoka, 1988)	1.613	0.085	0.365	1.222
Nevada sand (Lade <i>et al.</i> , 2014)	1.476	0.111	0.564	1.080
Leighton Buzzard sand (Yang <i>et al.</i> , 2016)	1.359	0.172	0.449	1.595

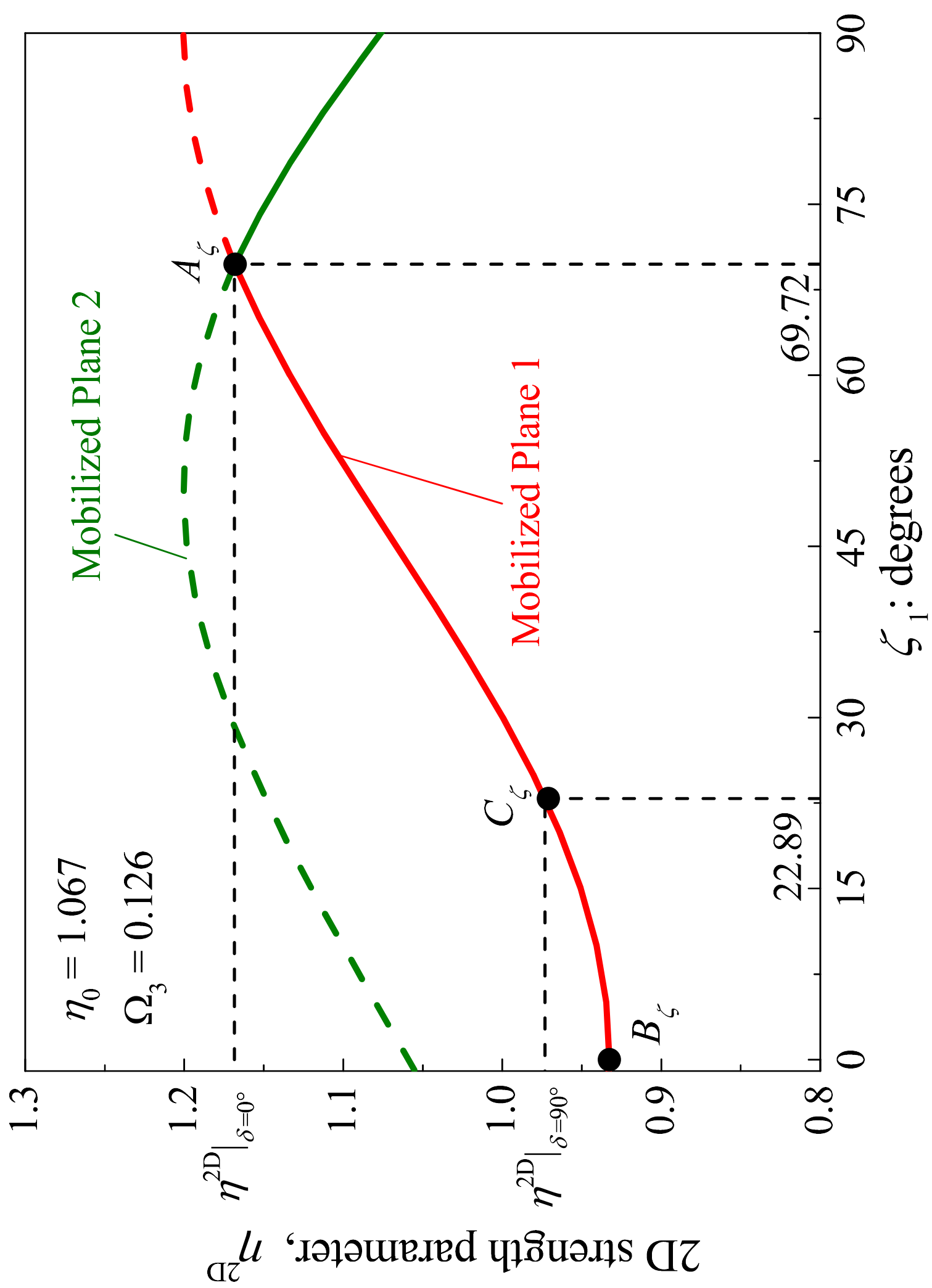


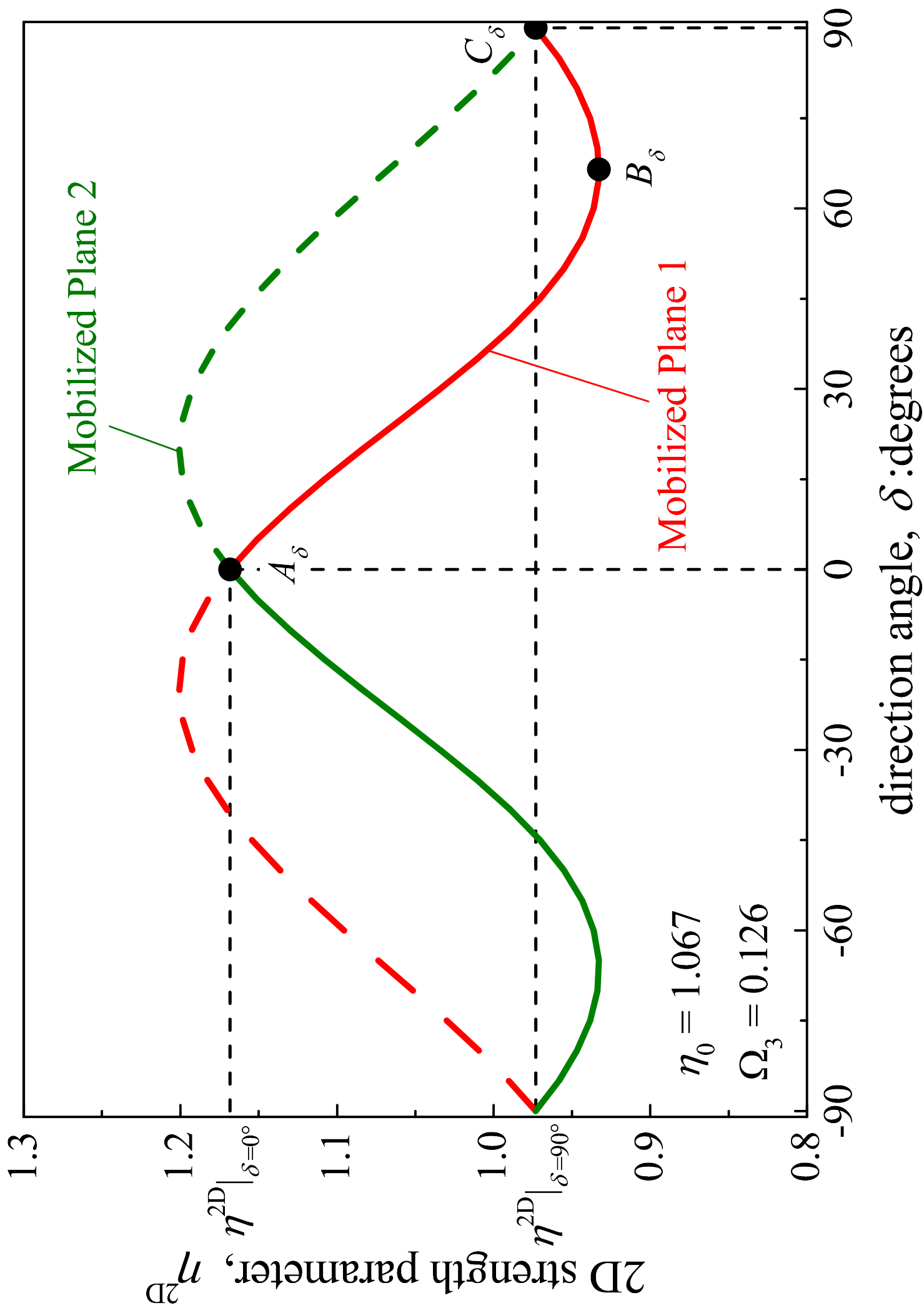


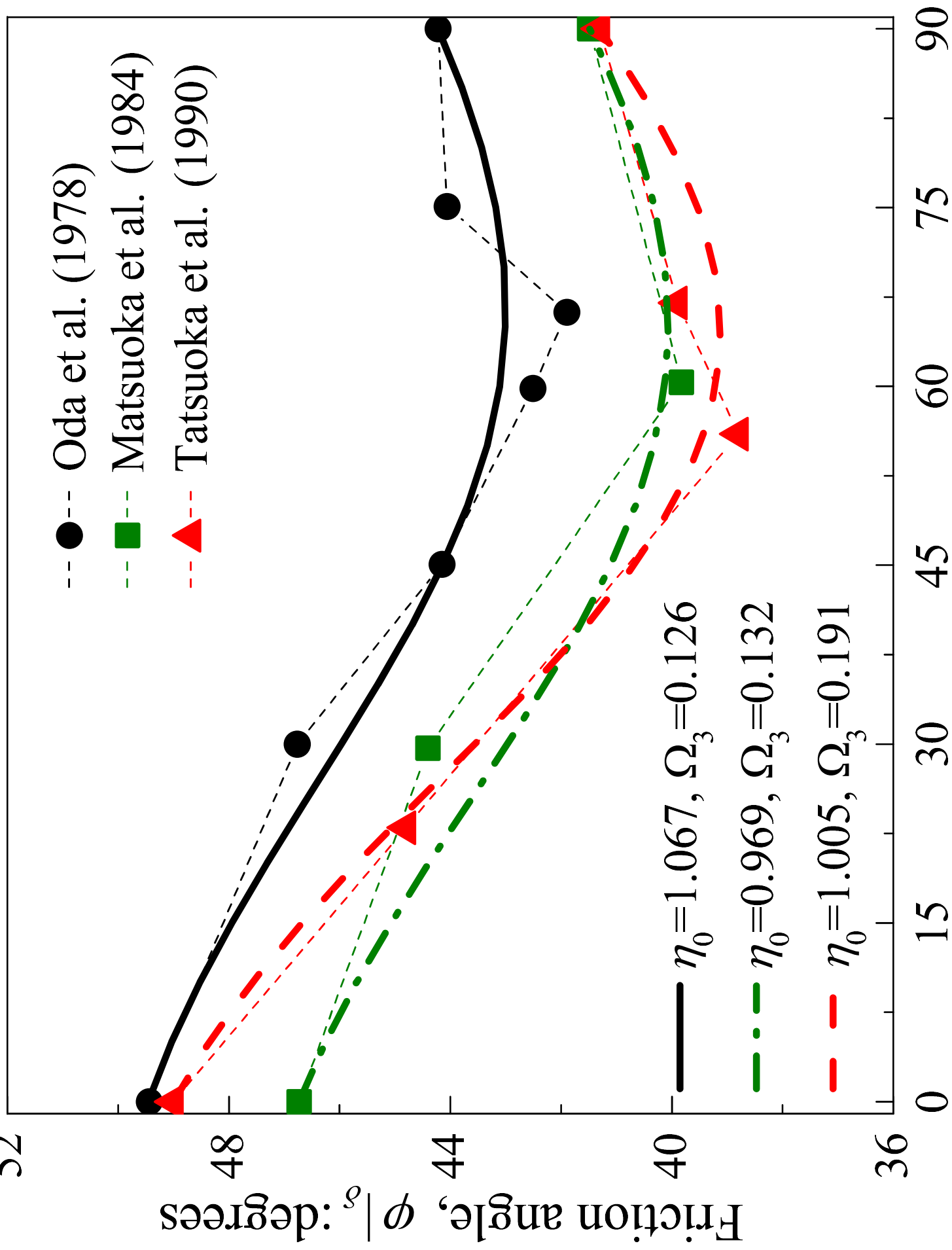




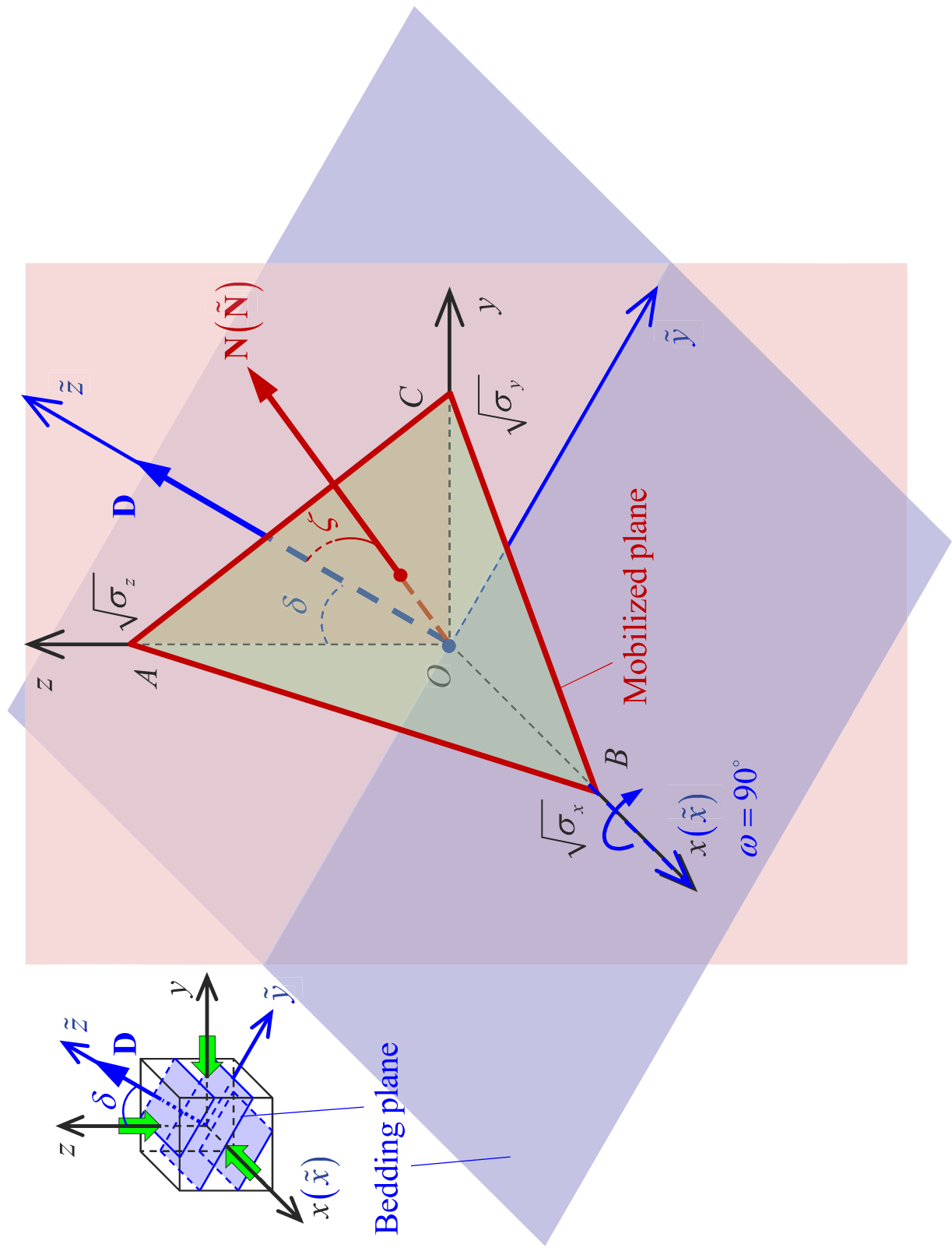


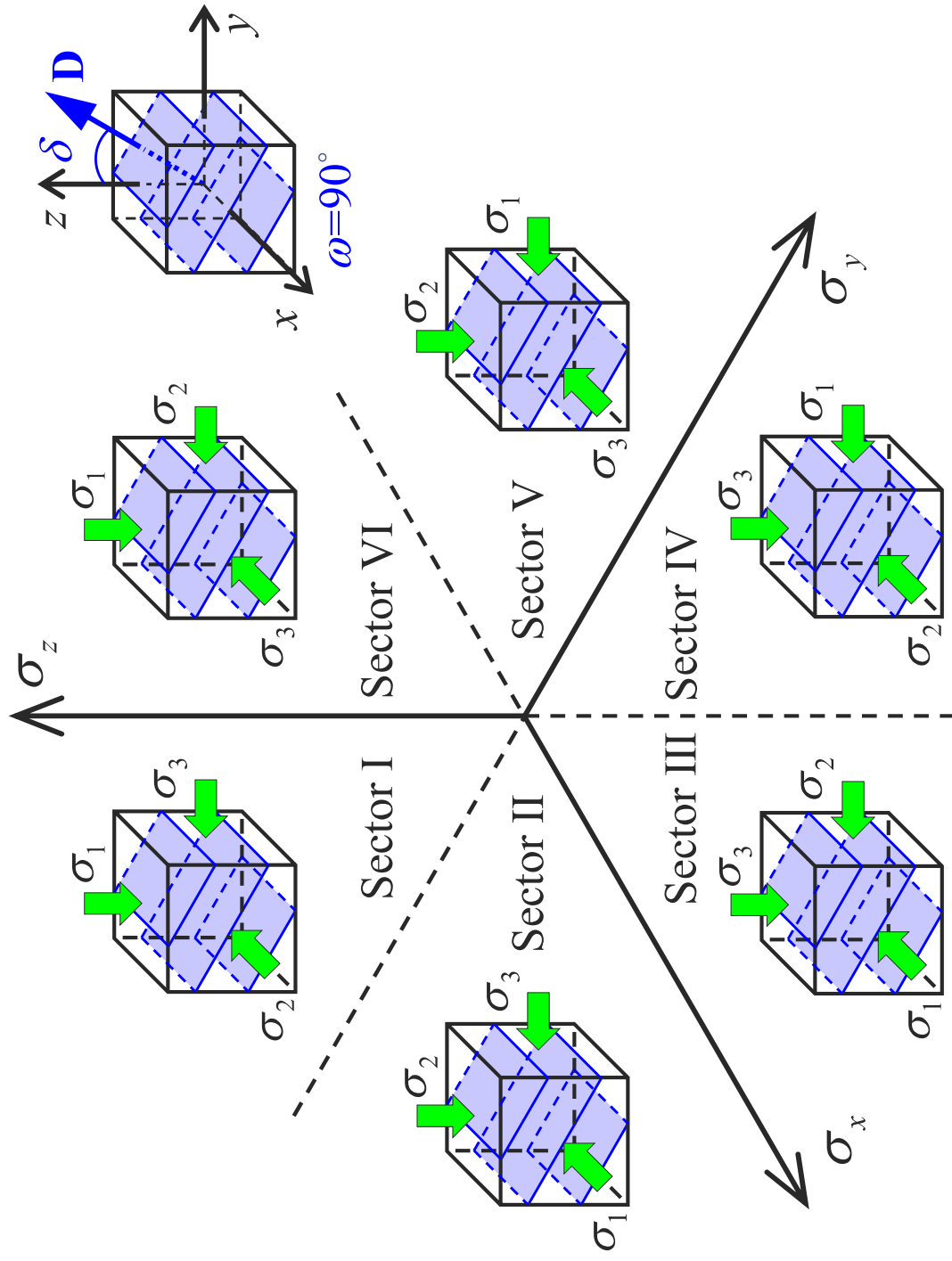


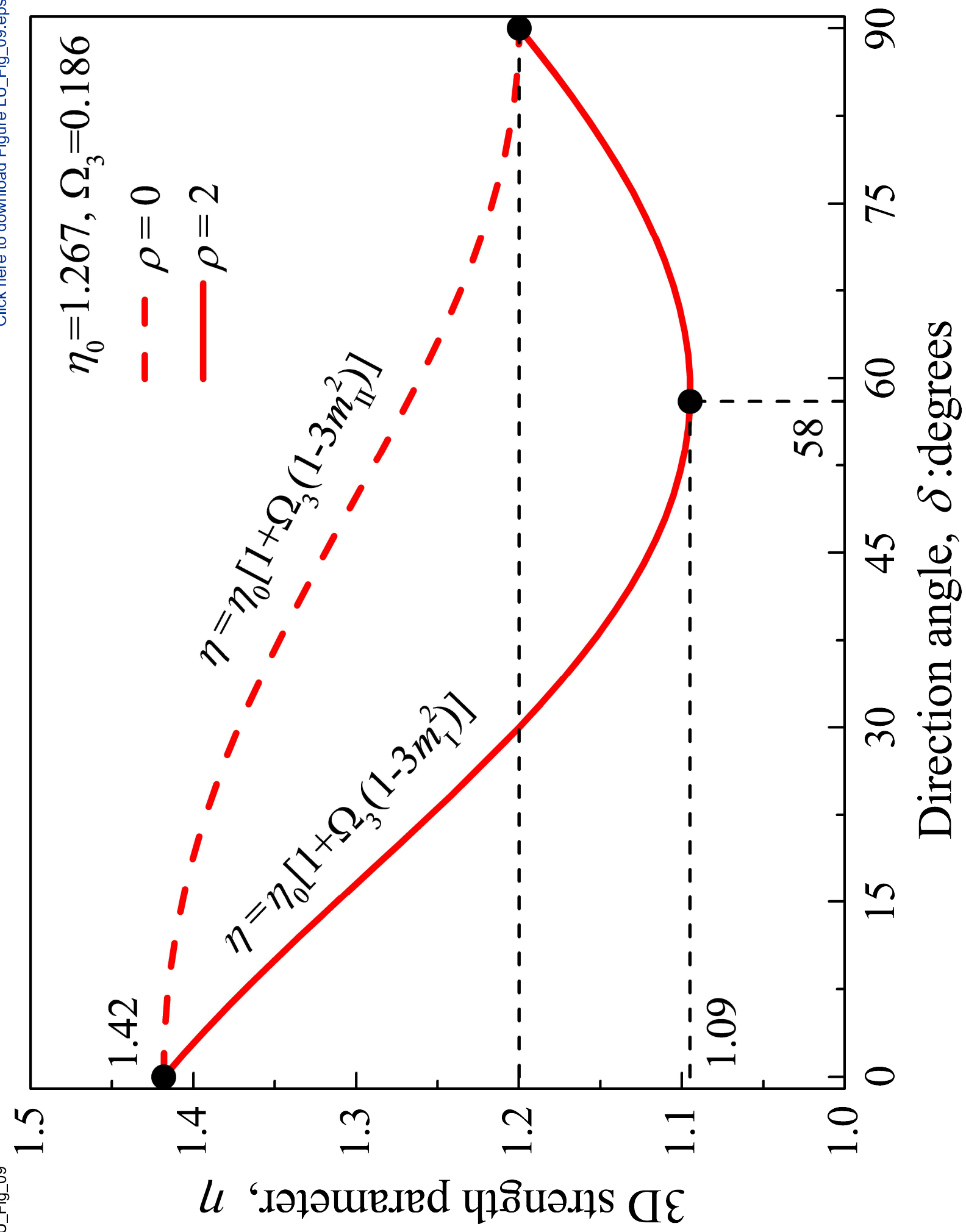


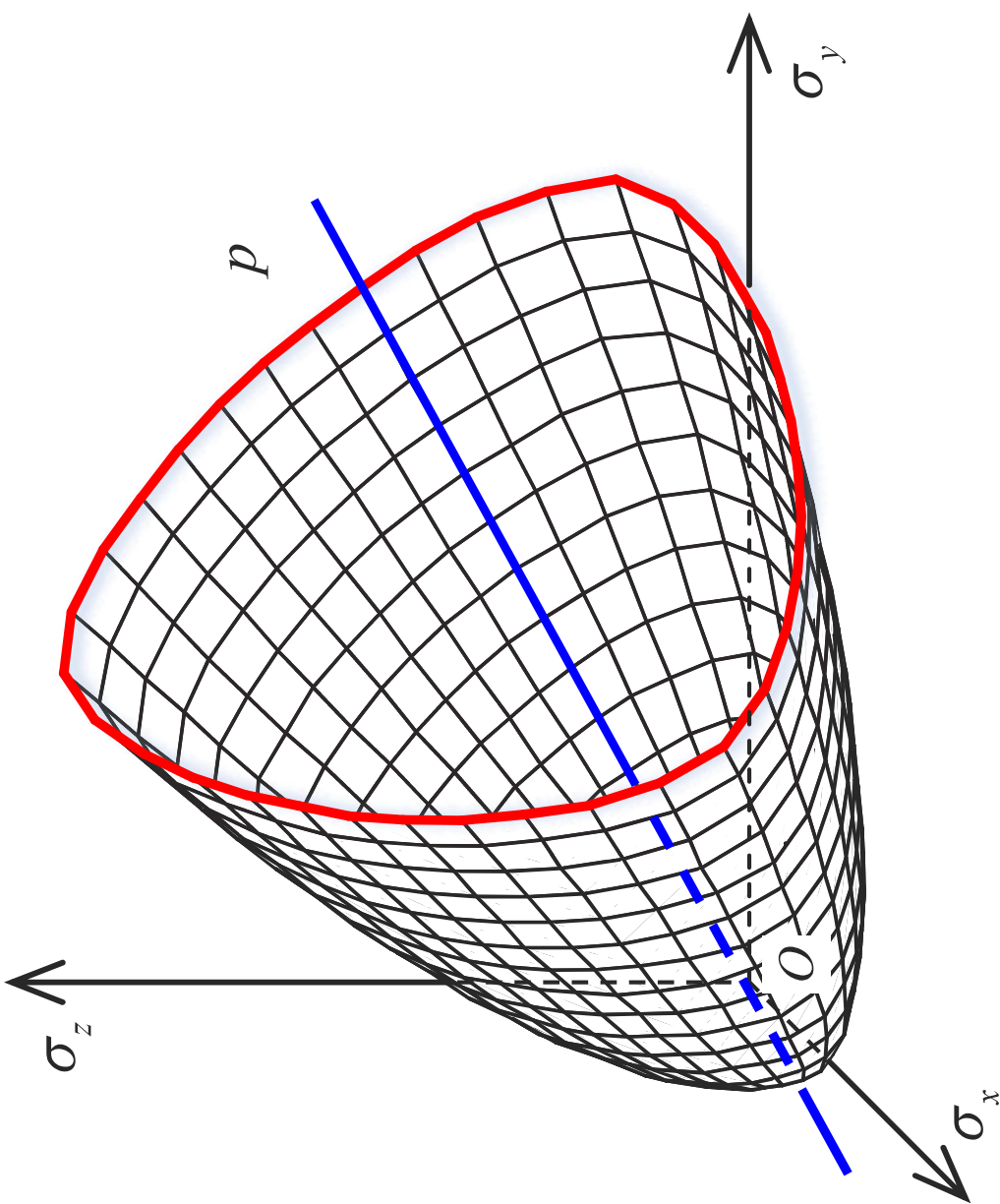


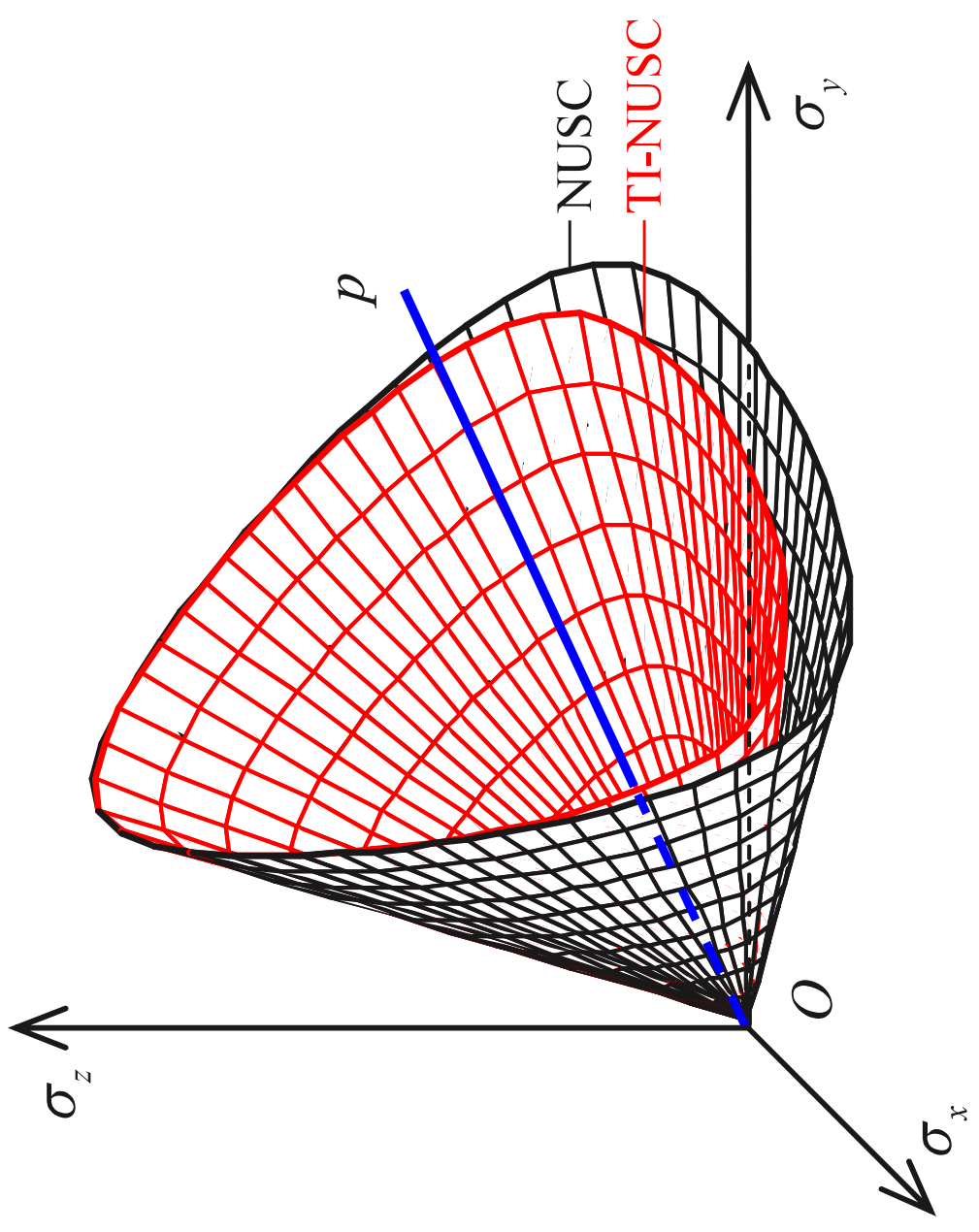
Direction angle, δ :degrees

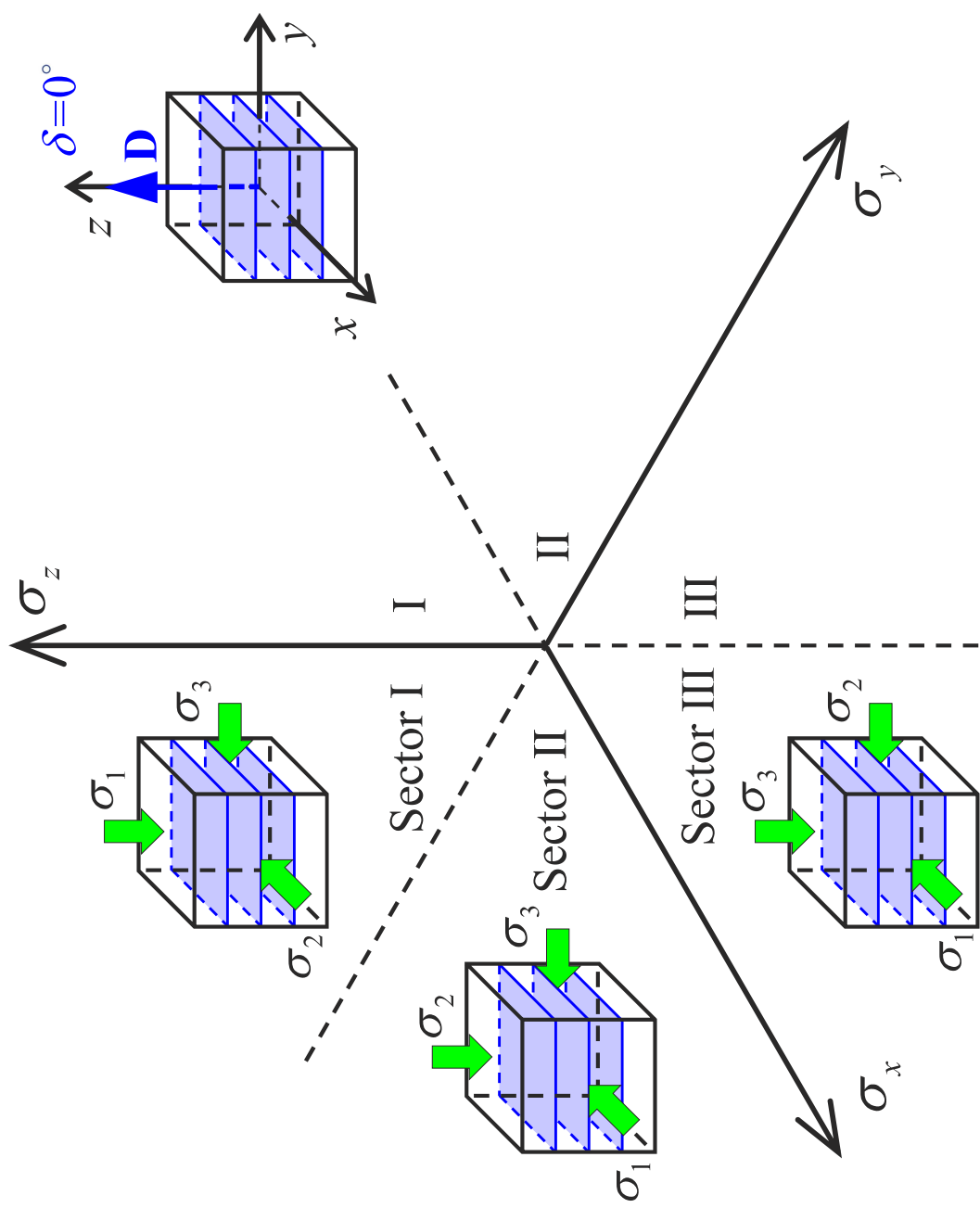


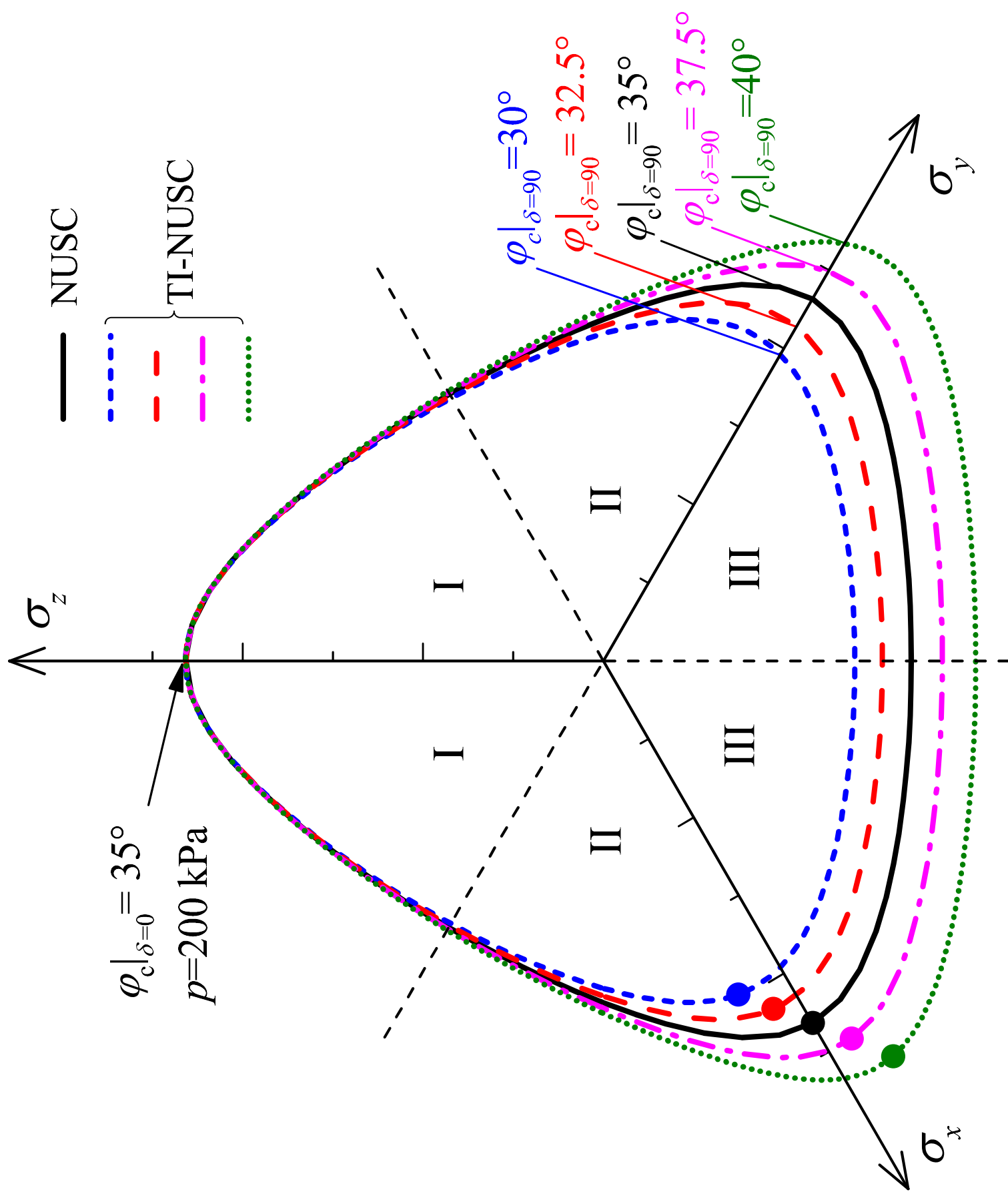


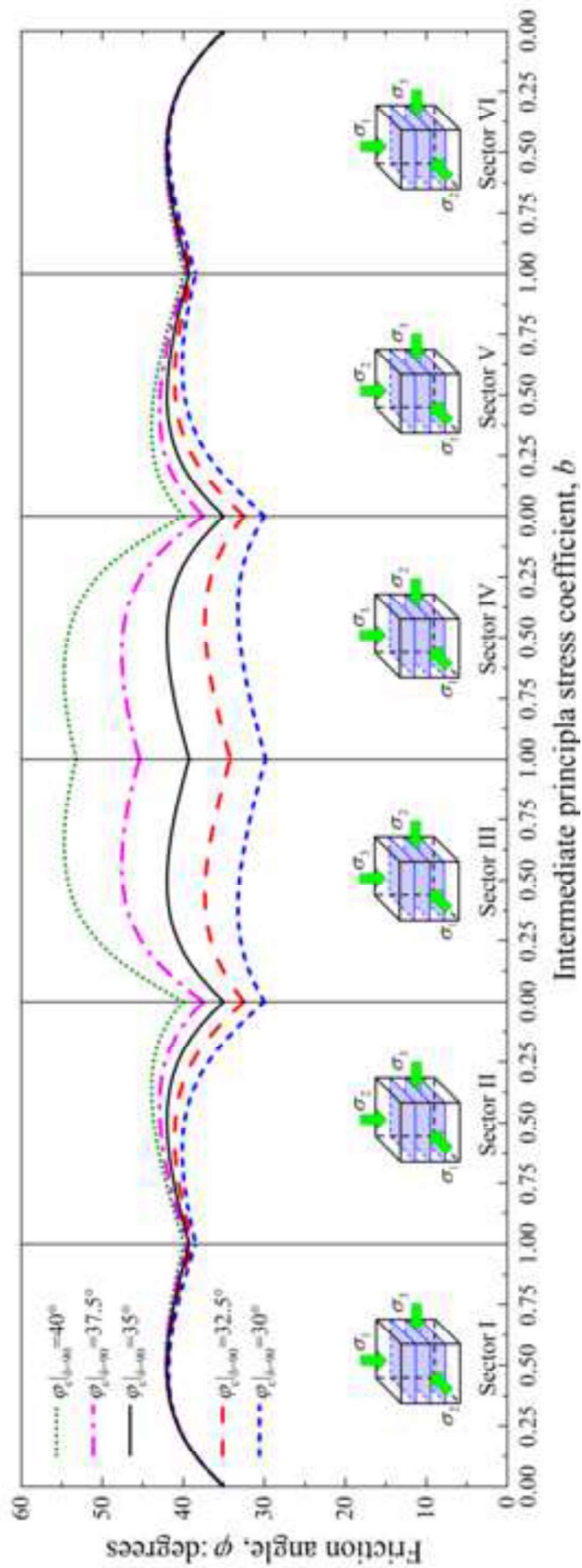


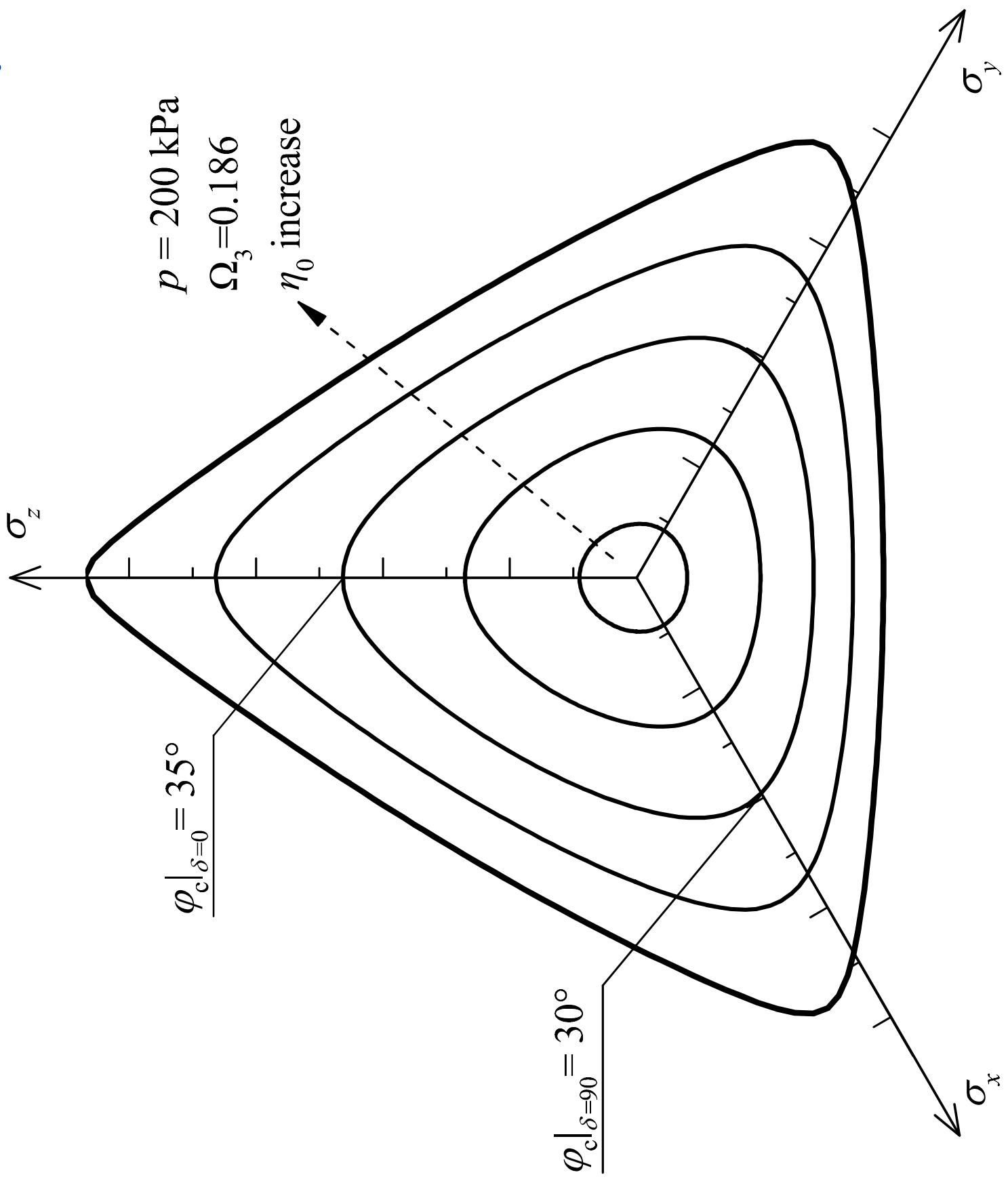


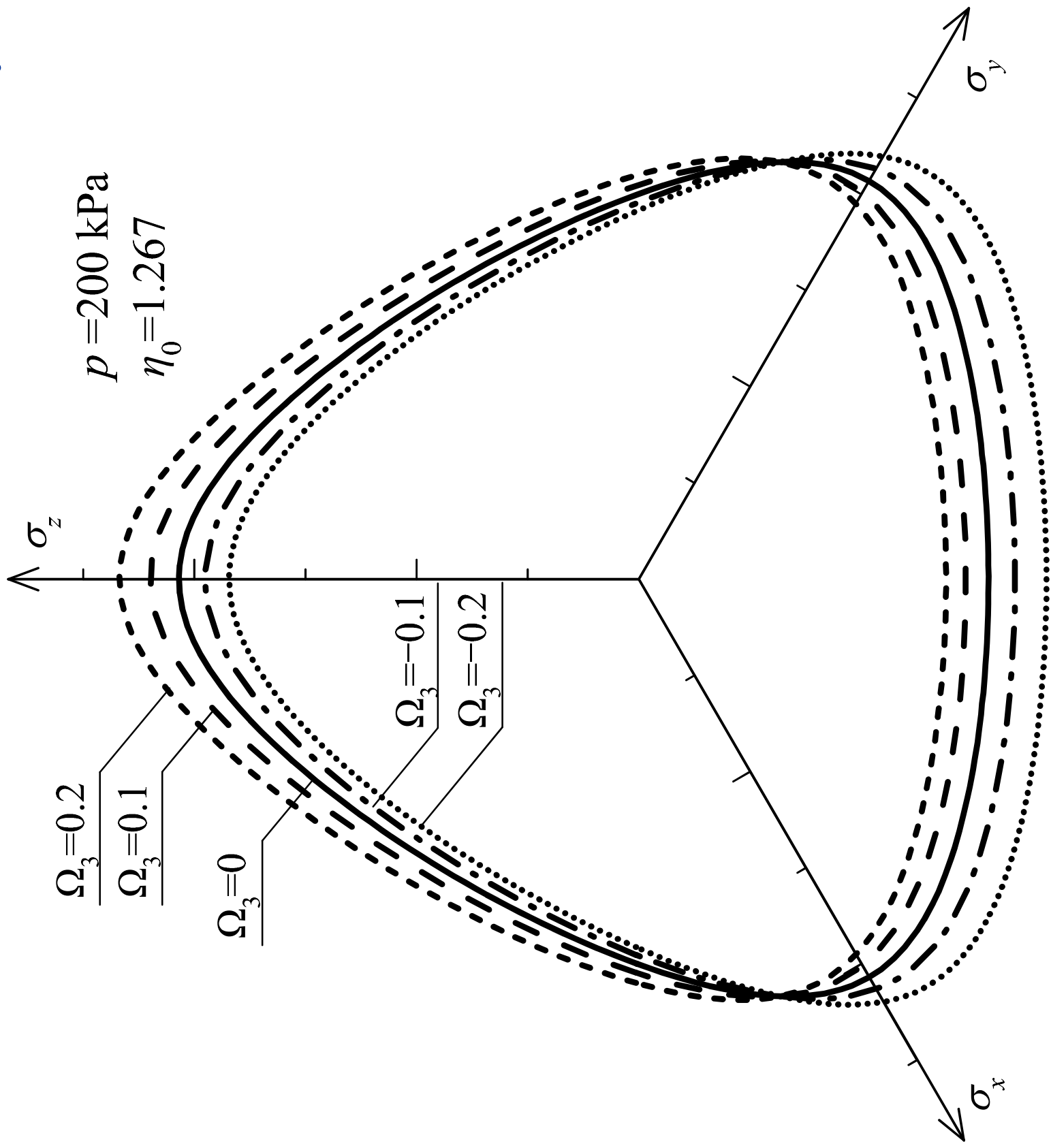












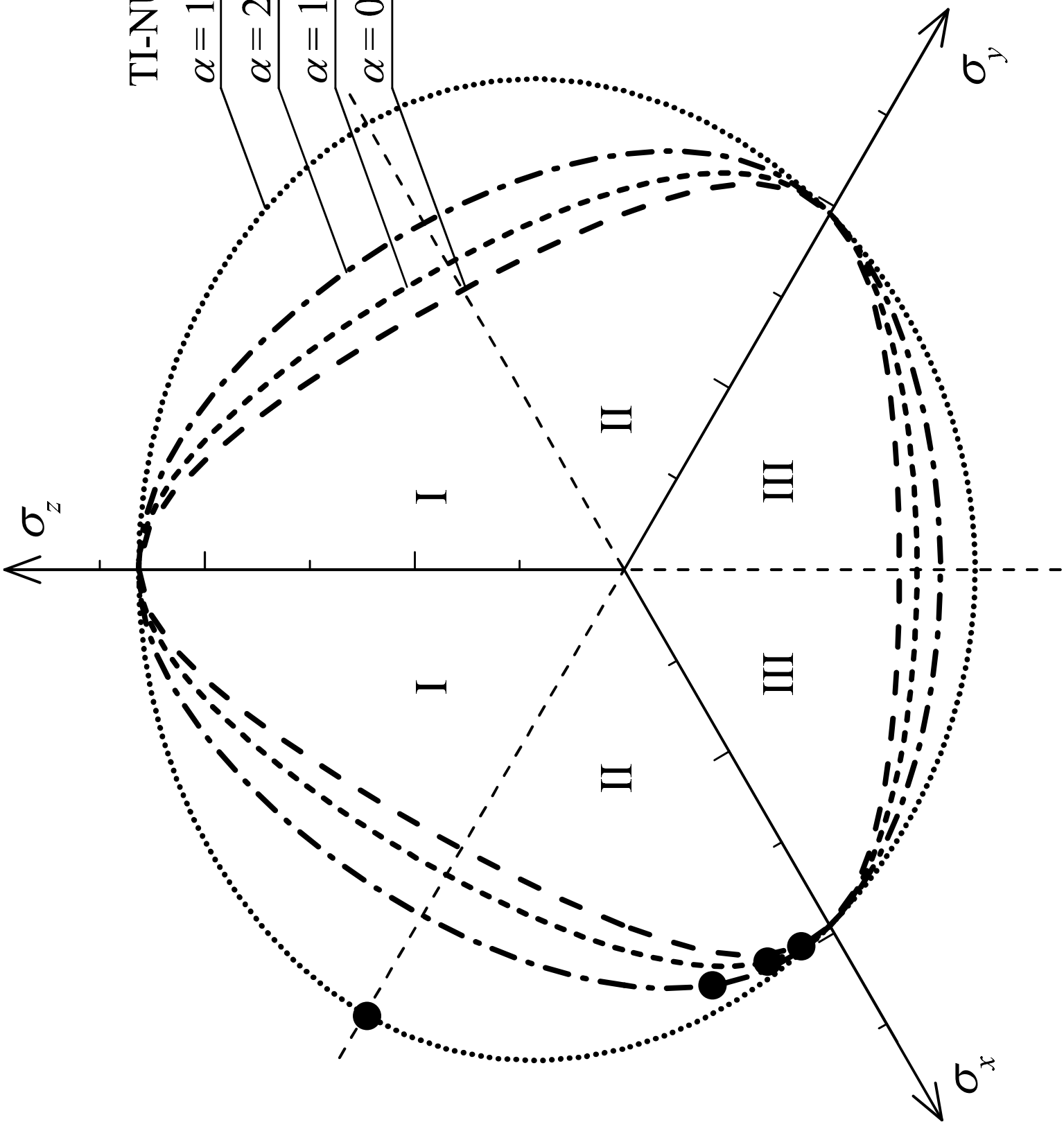
TI-NUSC

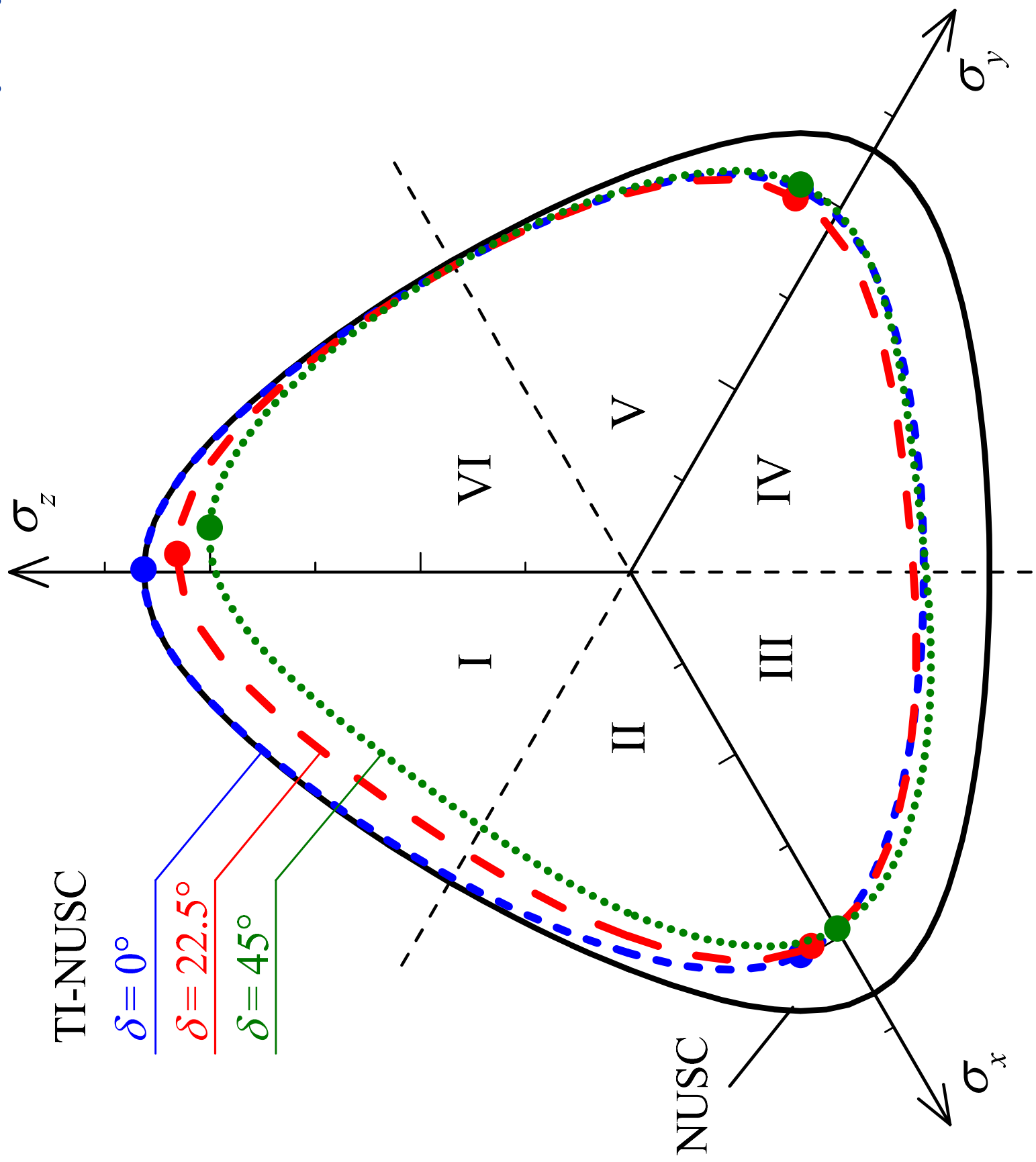
$$\alpha = 1$$

$$\alpha = 2/3$$

$$\alpha = 1/3$$

$$\alpha = 0$$





TI-NUSC

$\delta = 0^\circ$

$\delta = 22.5^\circ$

$\delta = 45^\circ$

NUSC

I

II

III

IV

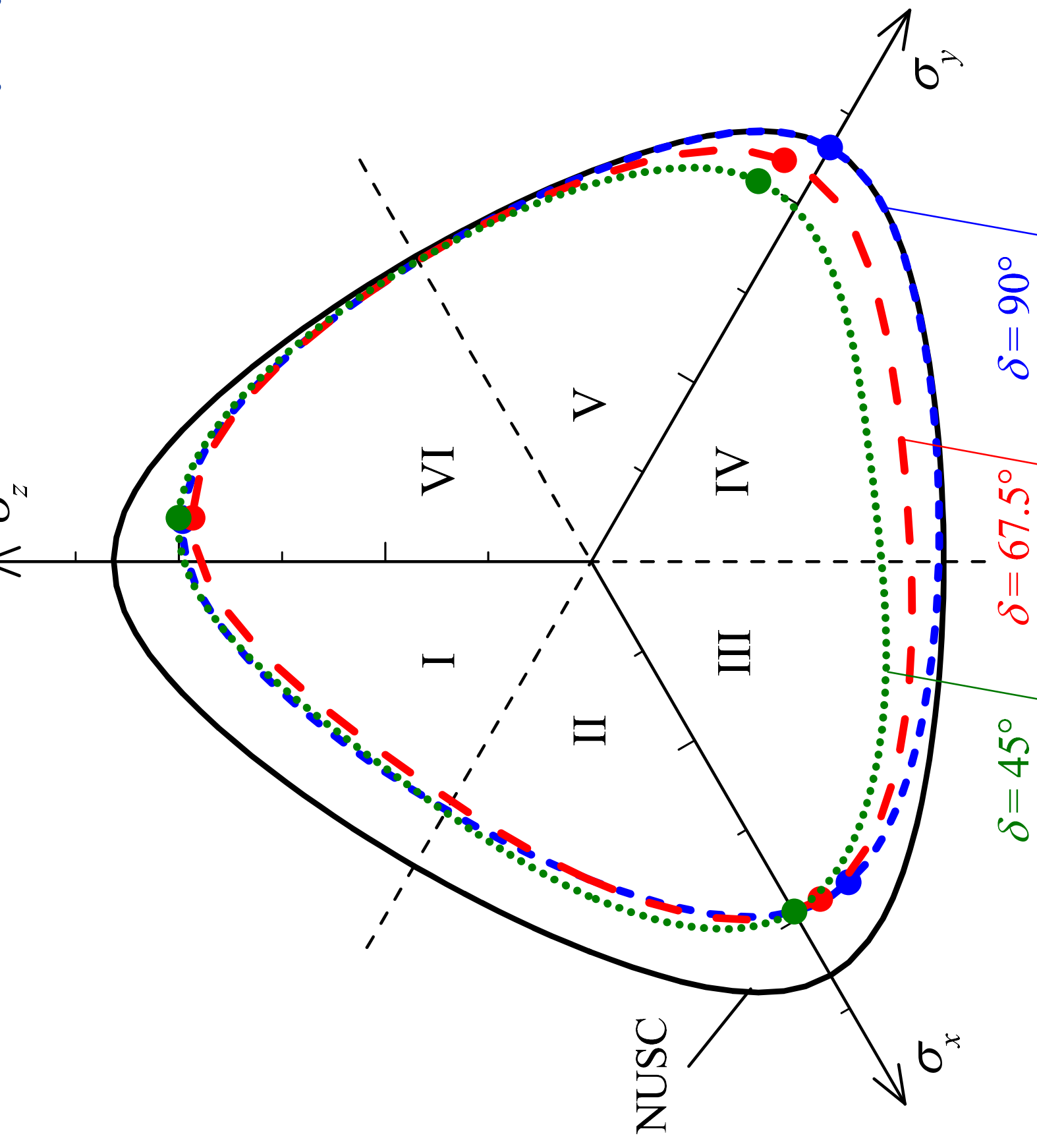
V

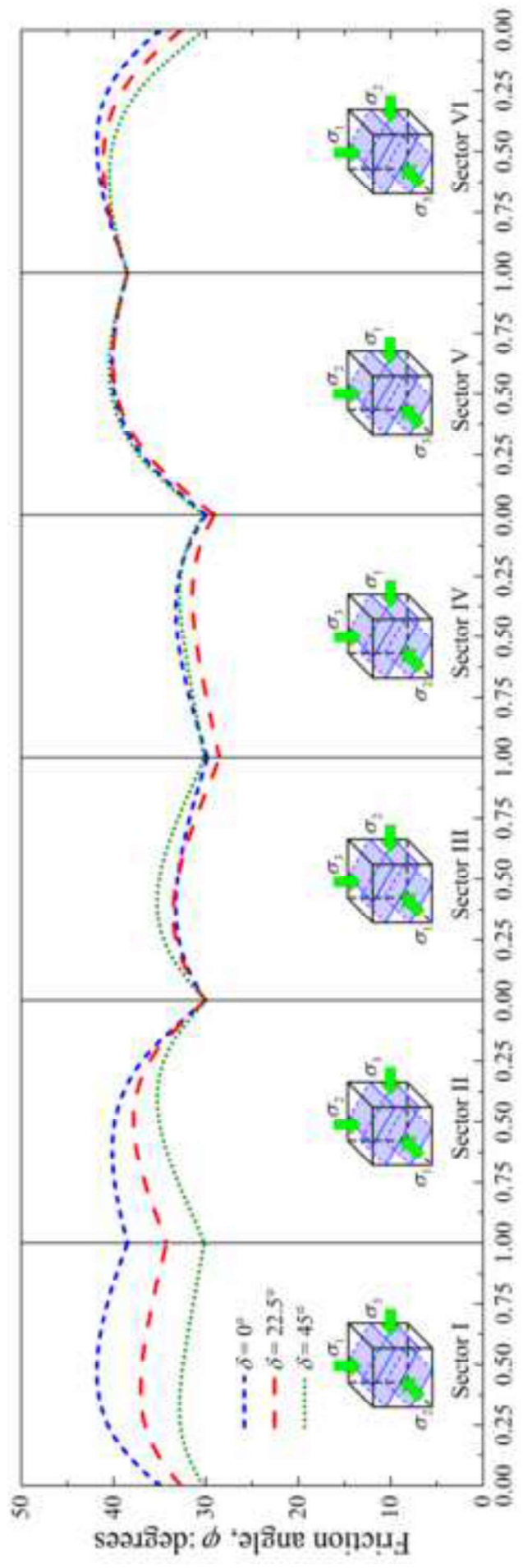
VI

σ_z

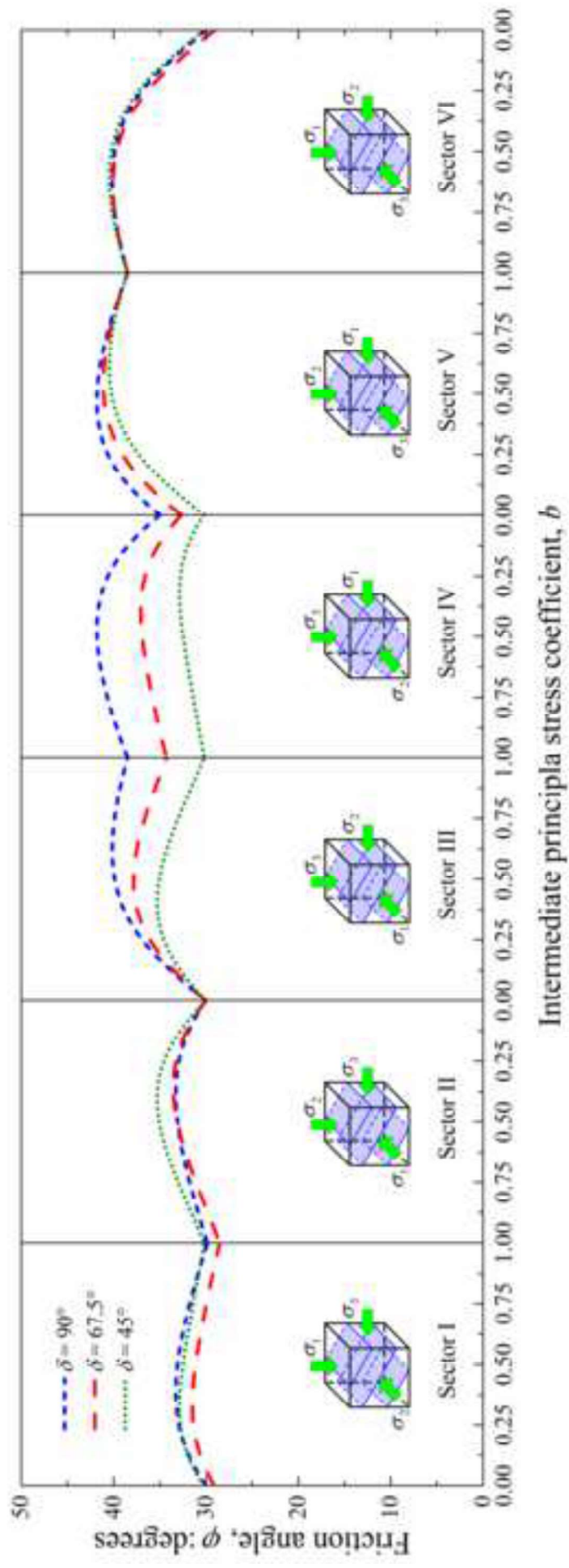
σ_x

σ_y

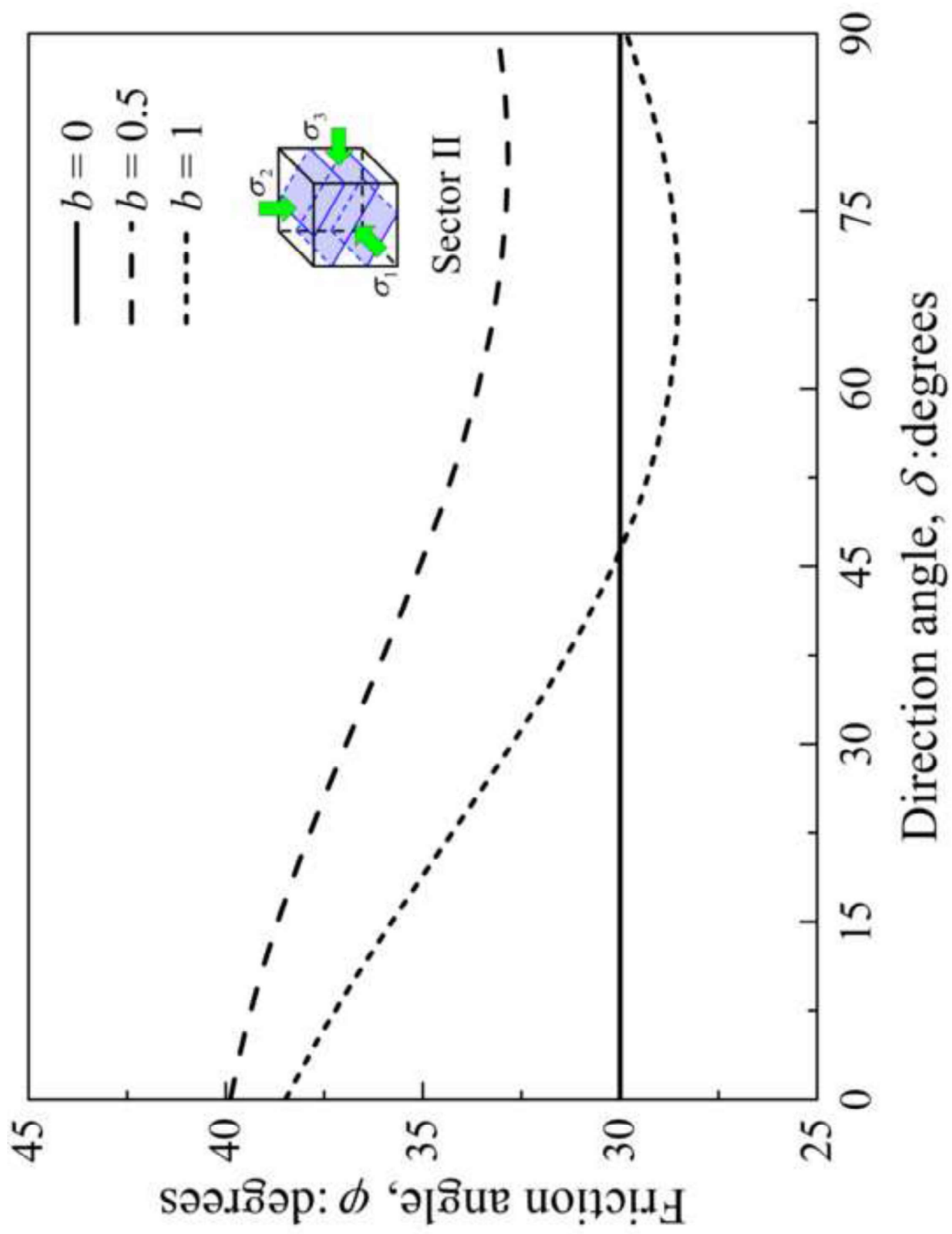


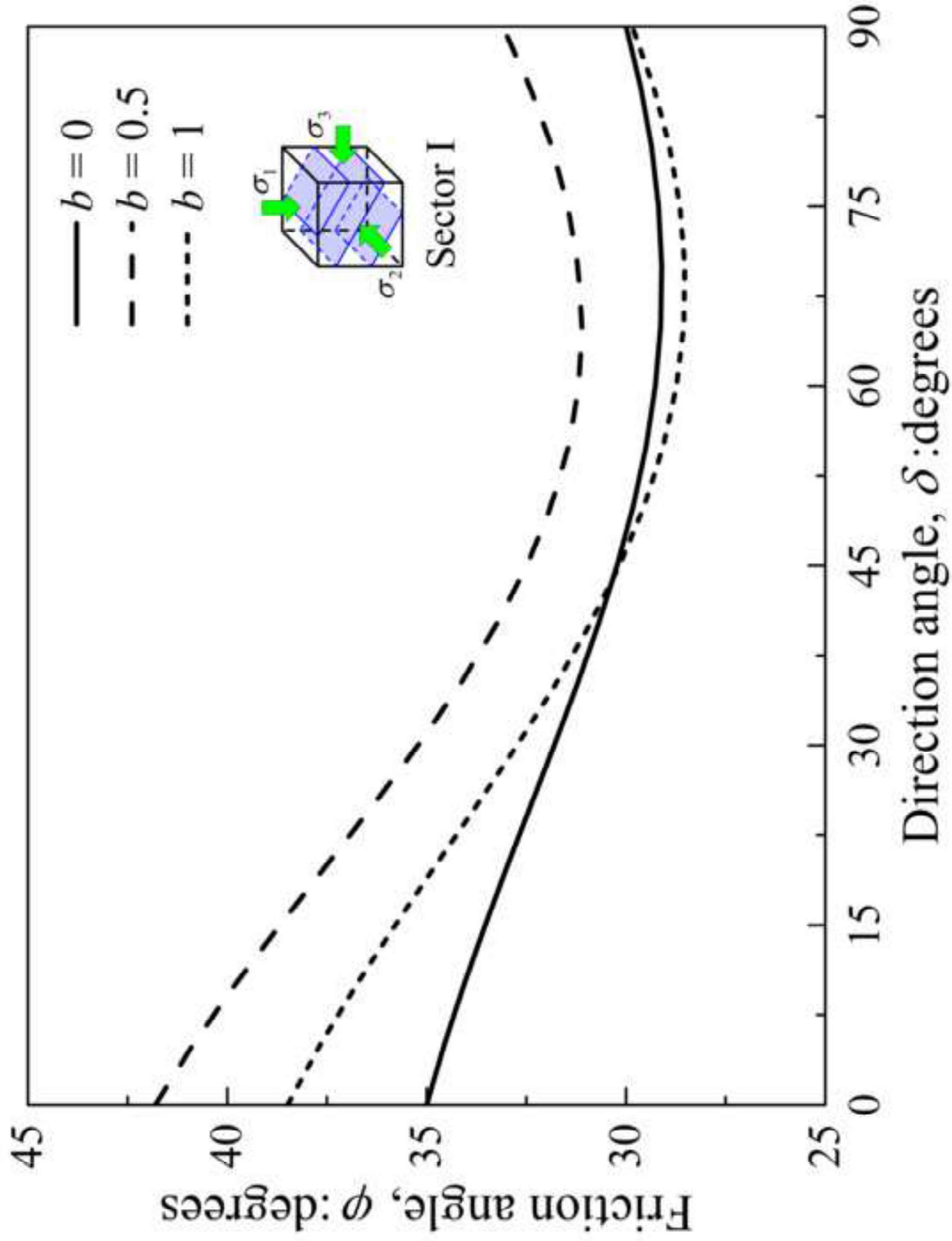


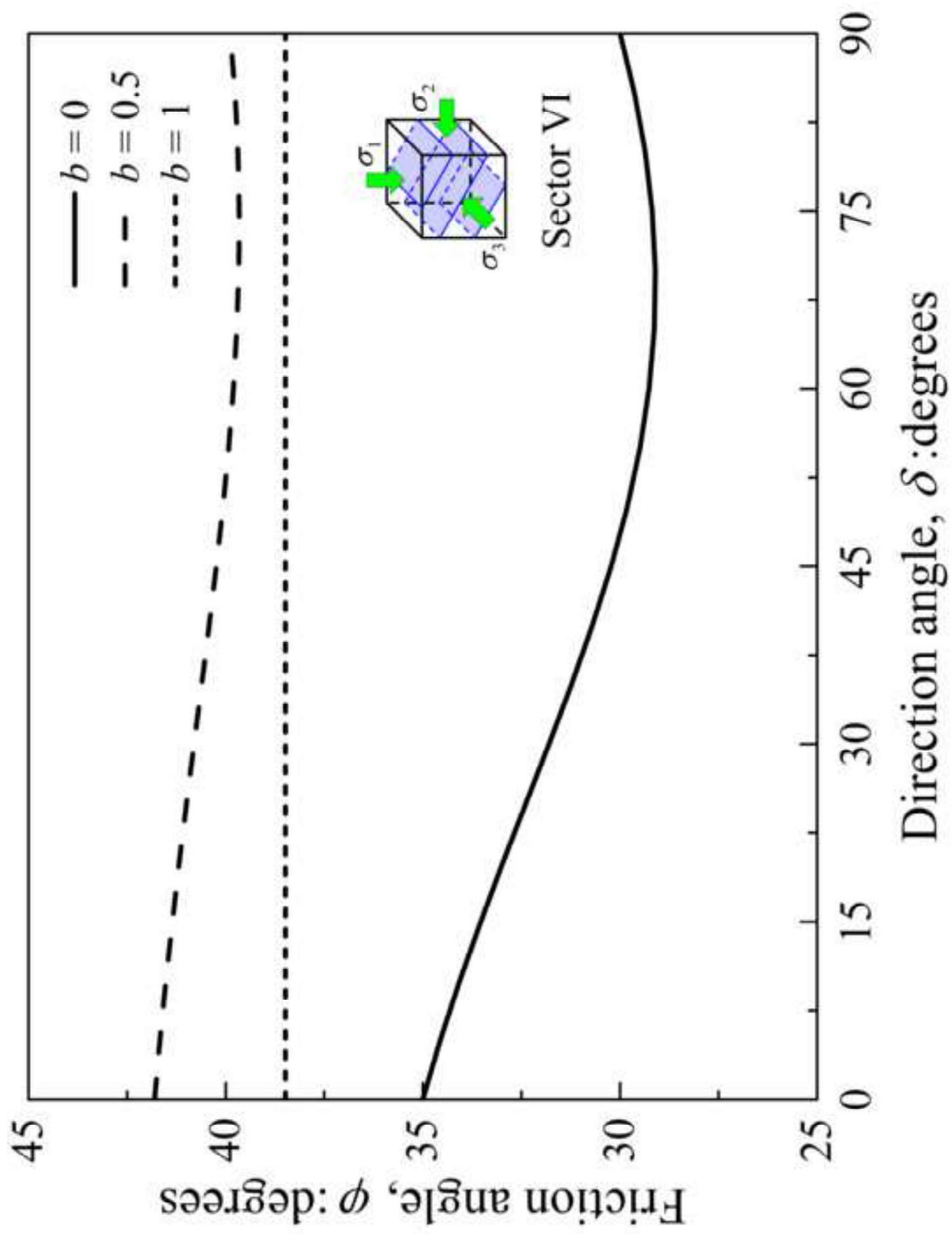
Intermediate principal stress coefficient, b



Intermediate principal stress coefficient, b







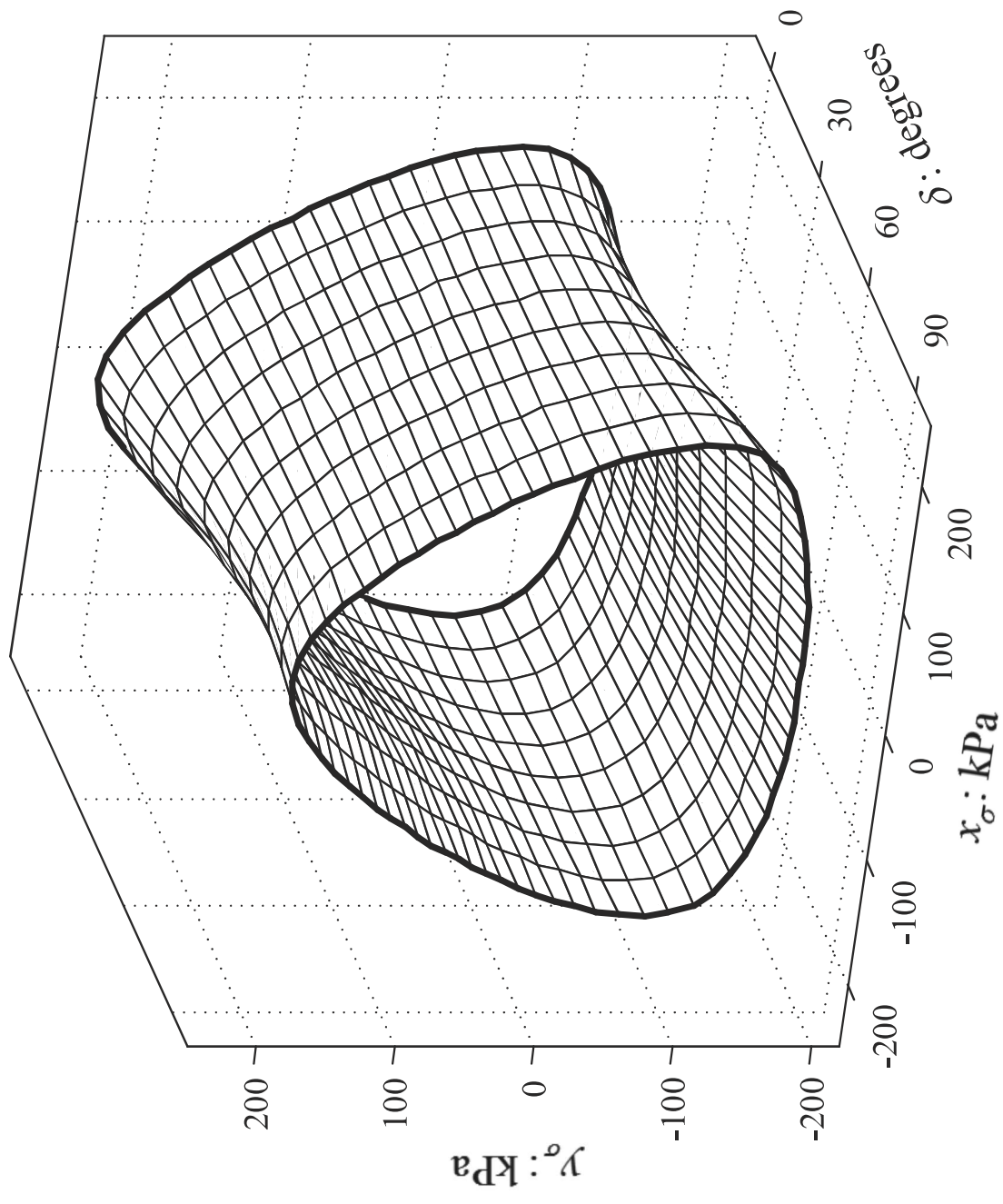
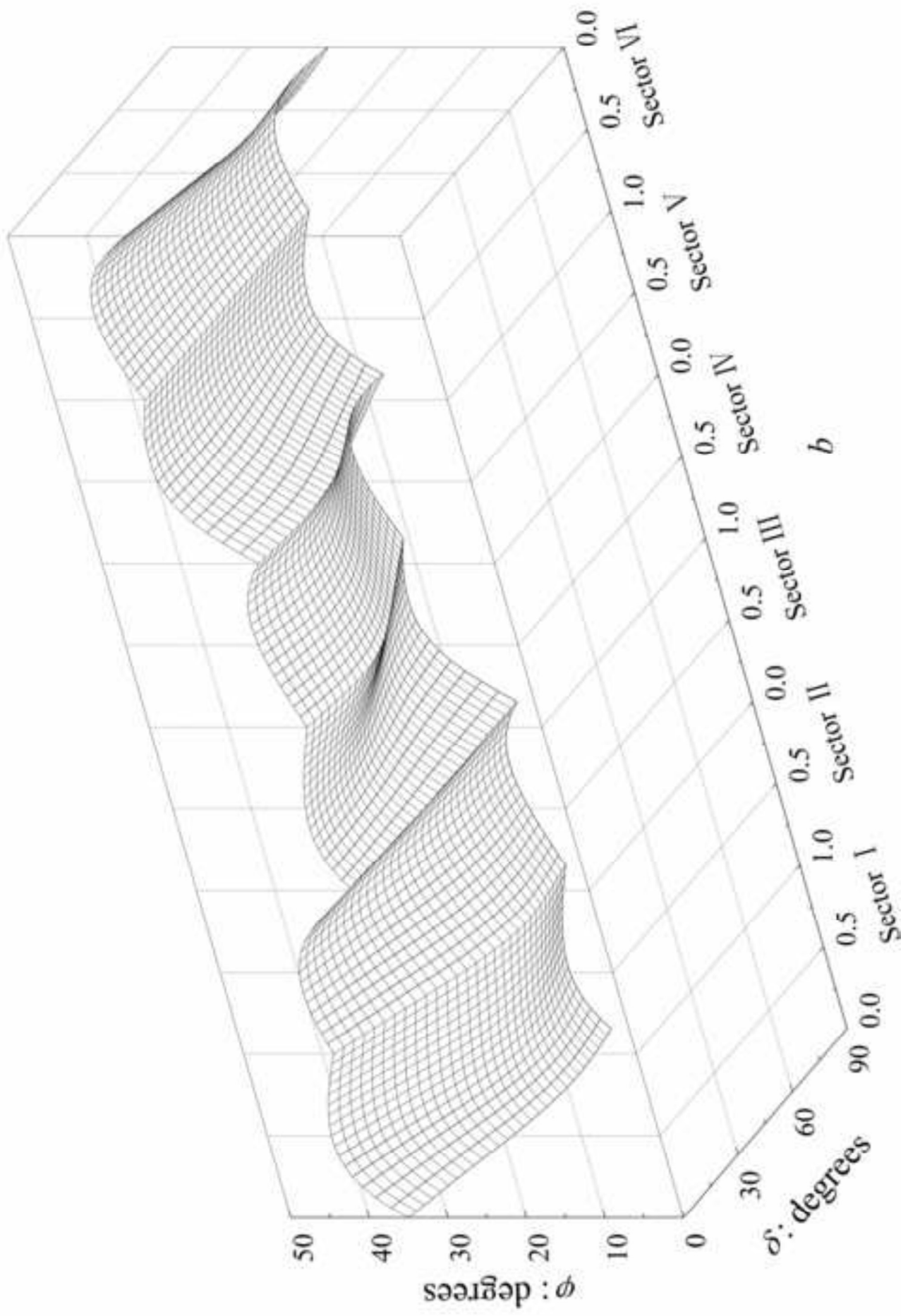
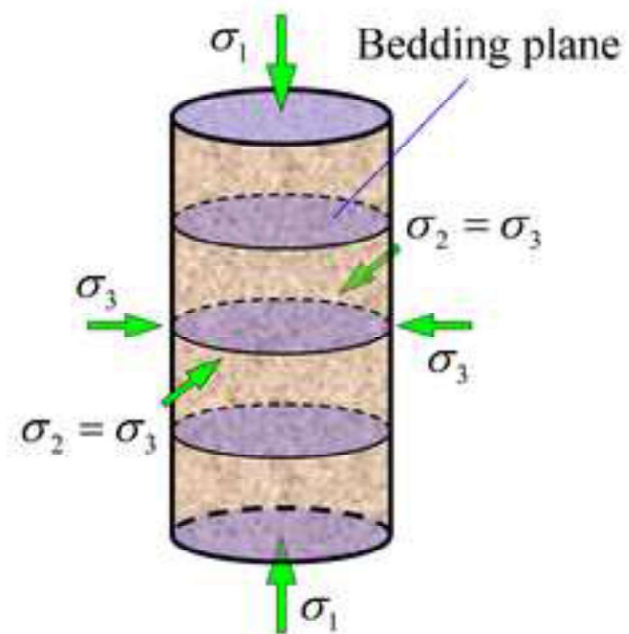
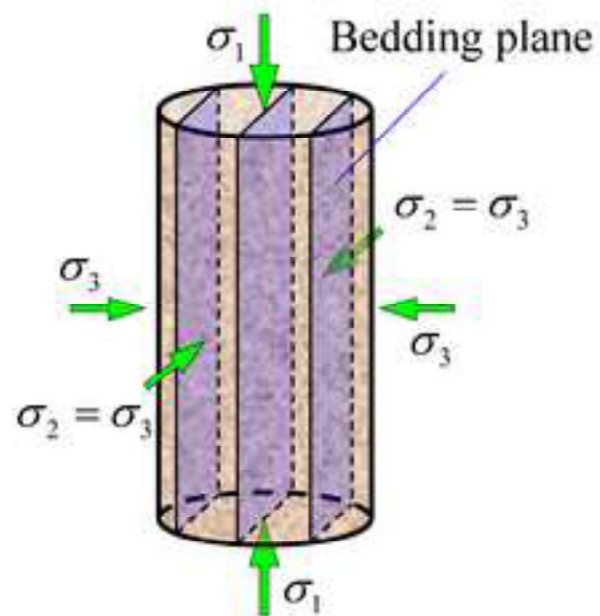
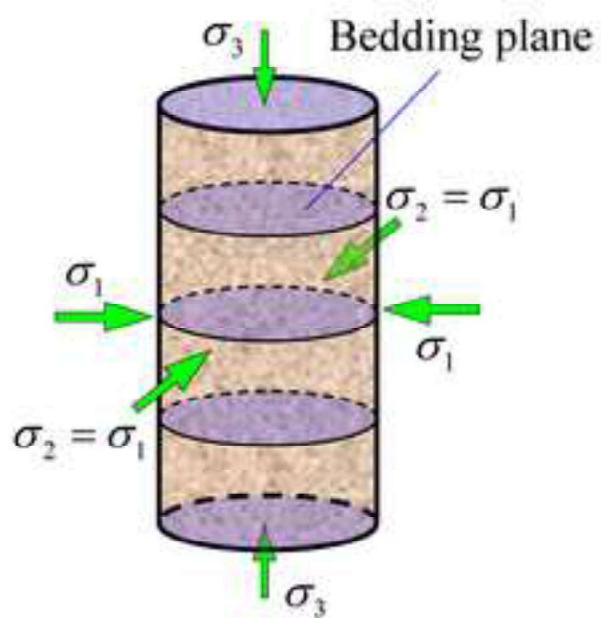


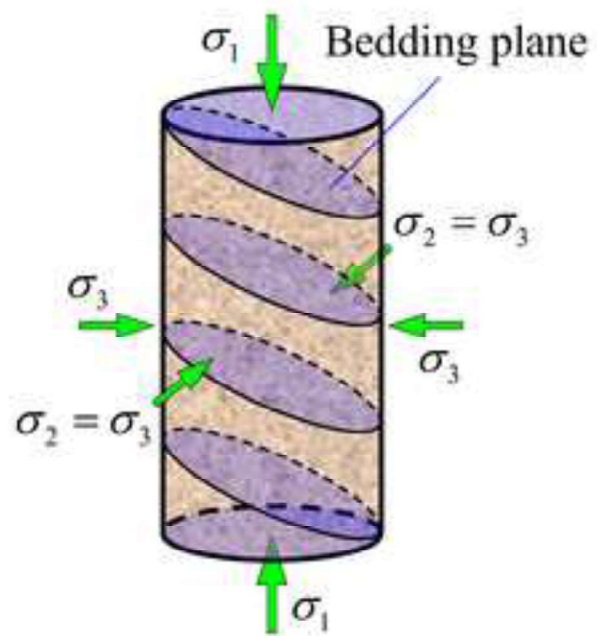
Fig. 1 Strength evolution with b and δ at $p = 200$ kPa

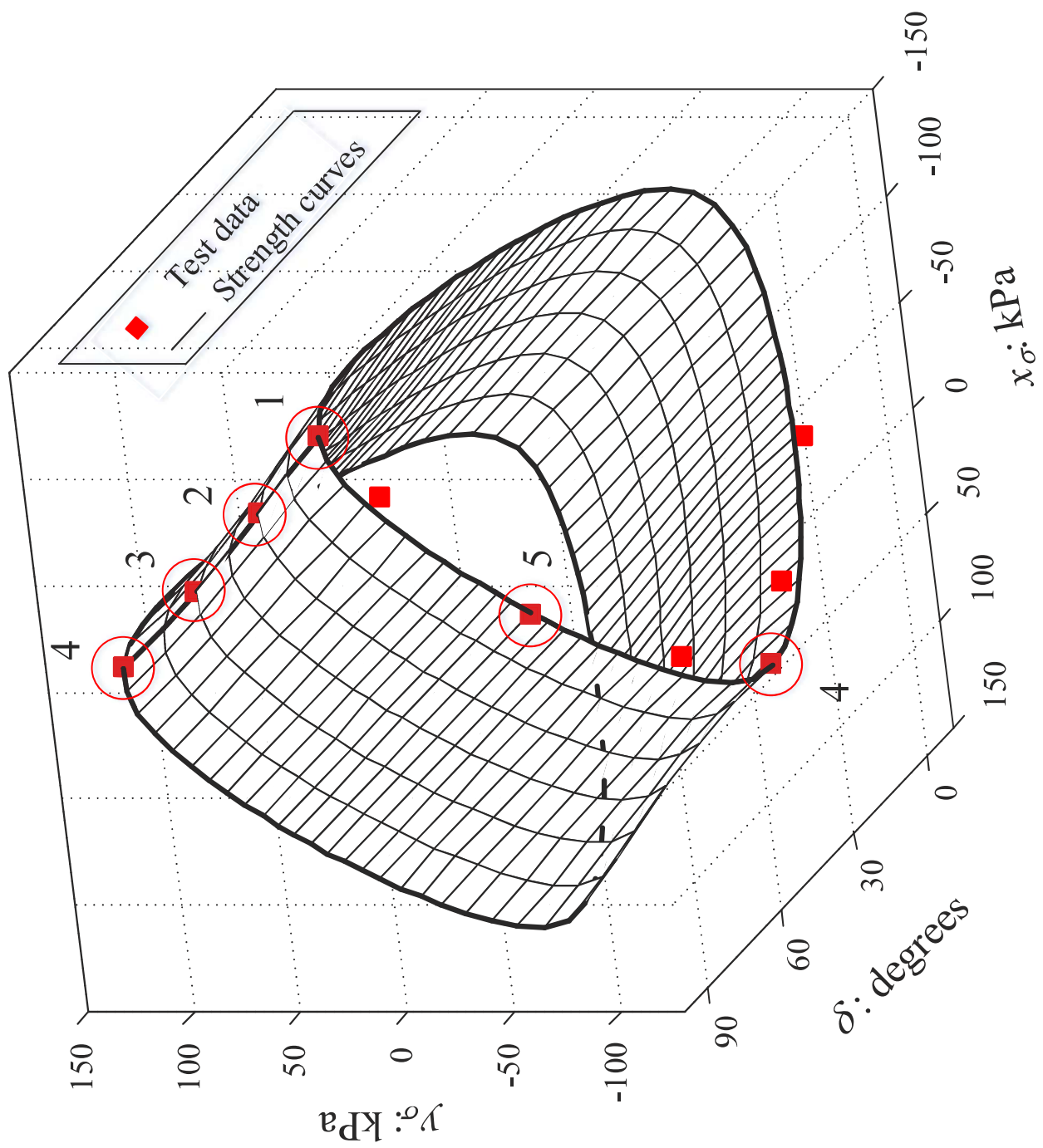


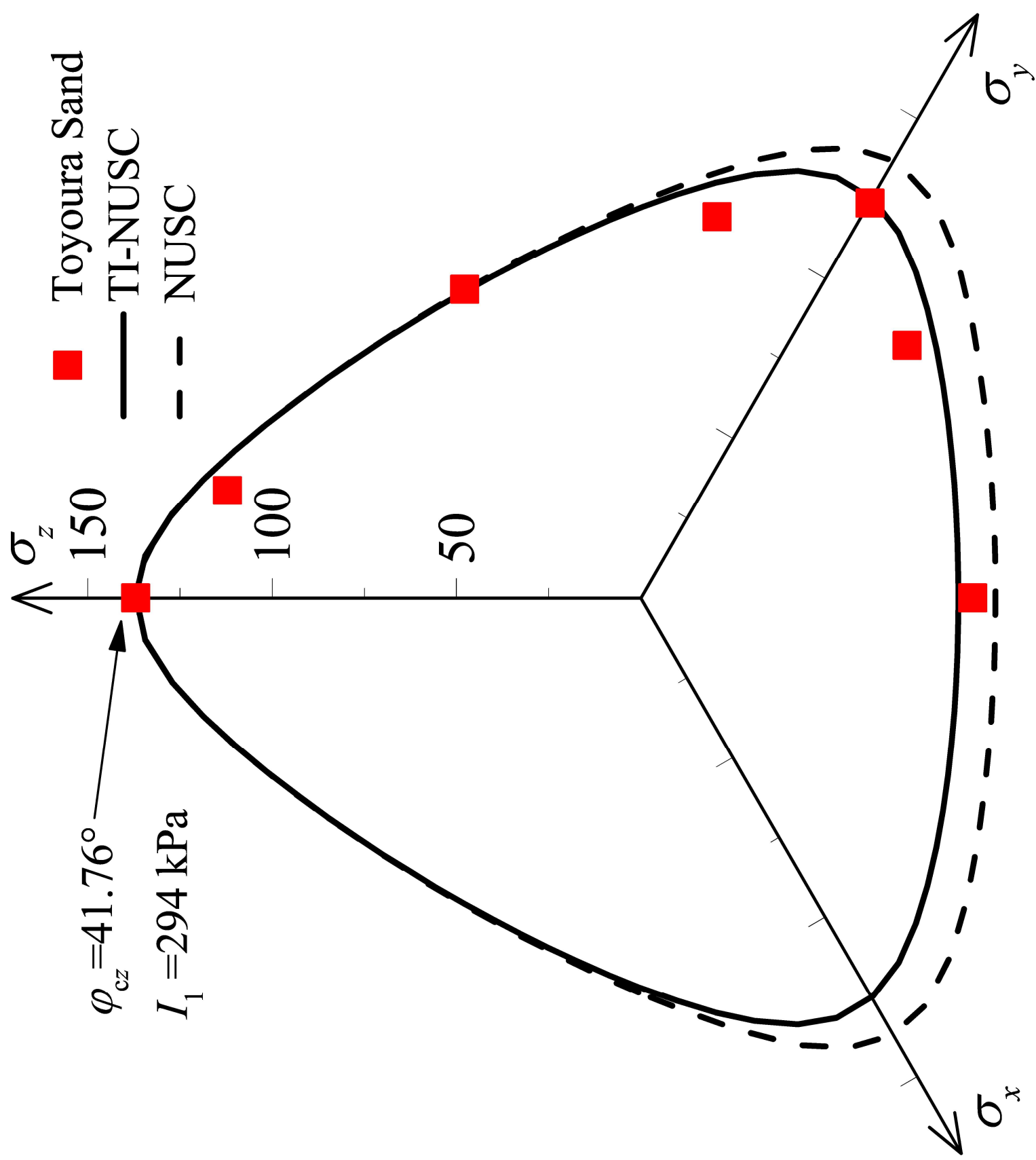


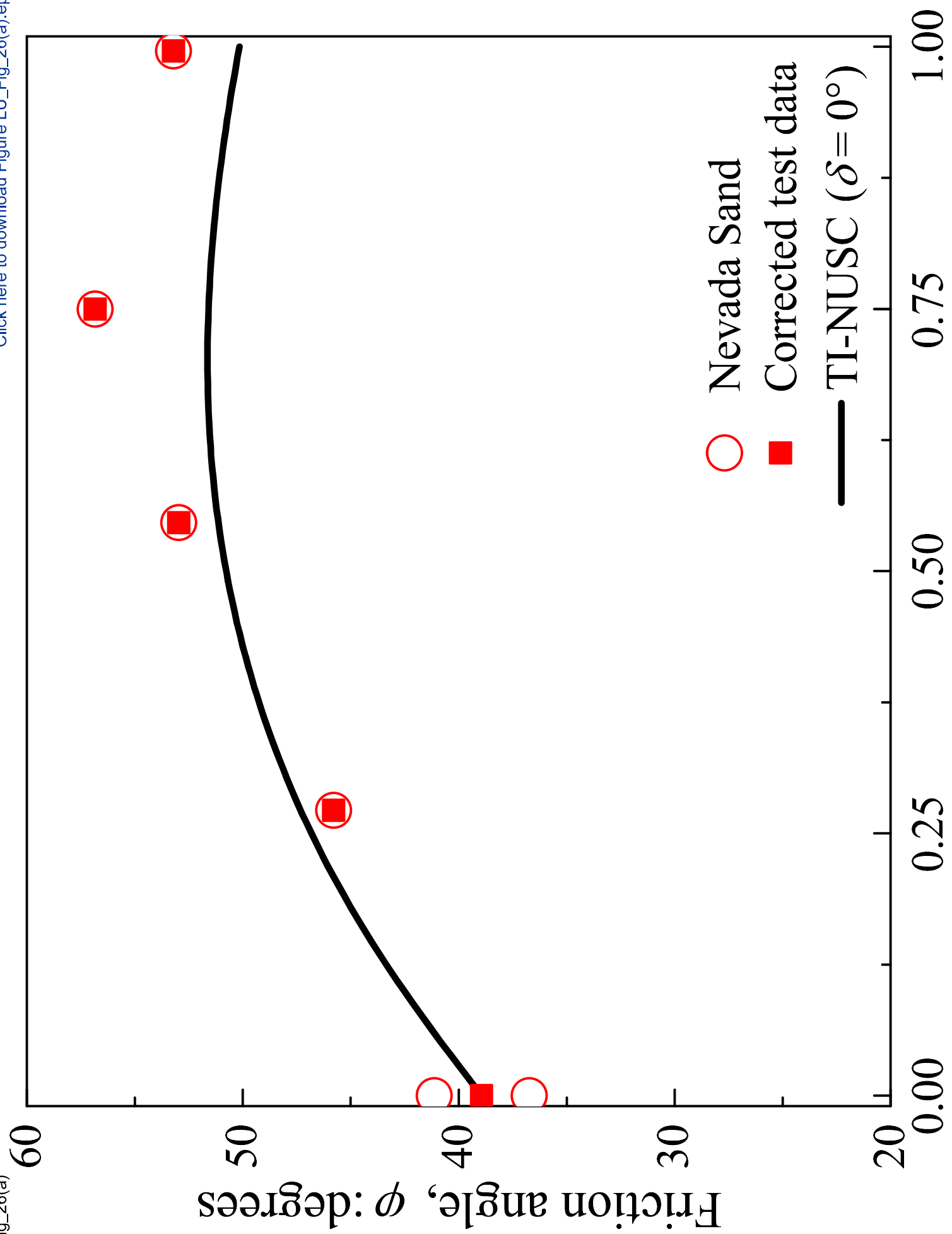




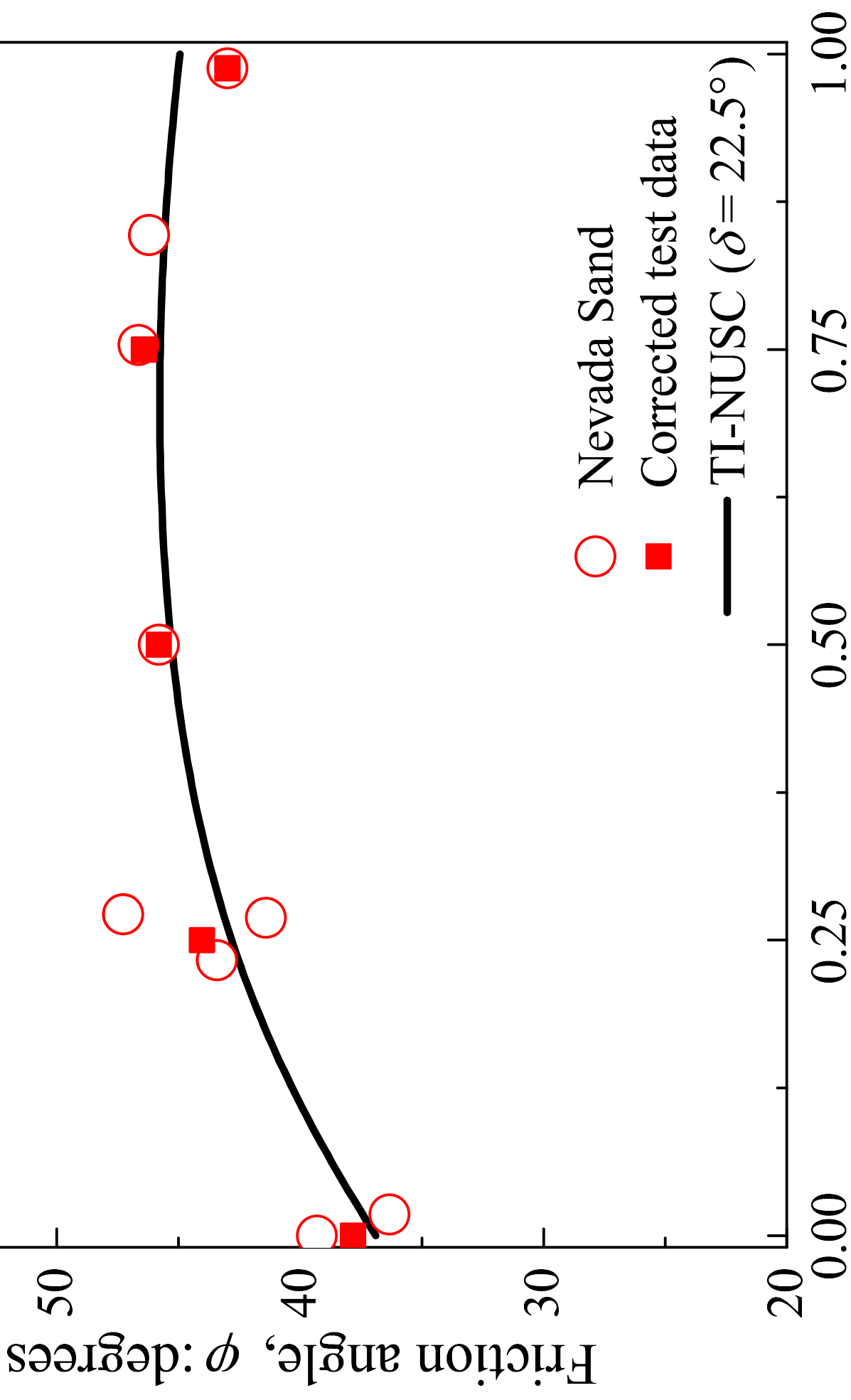




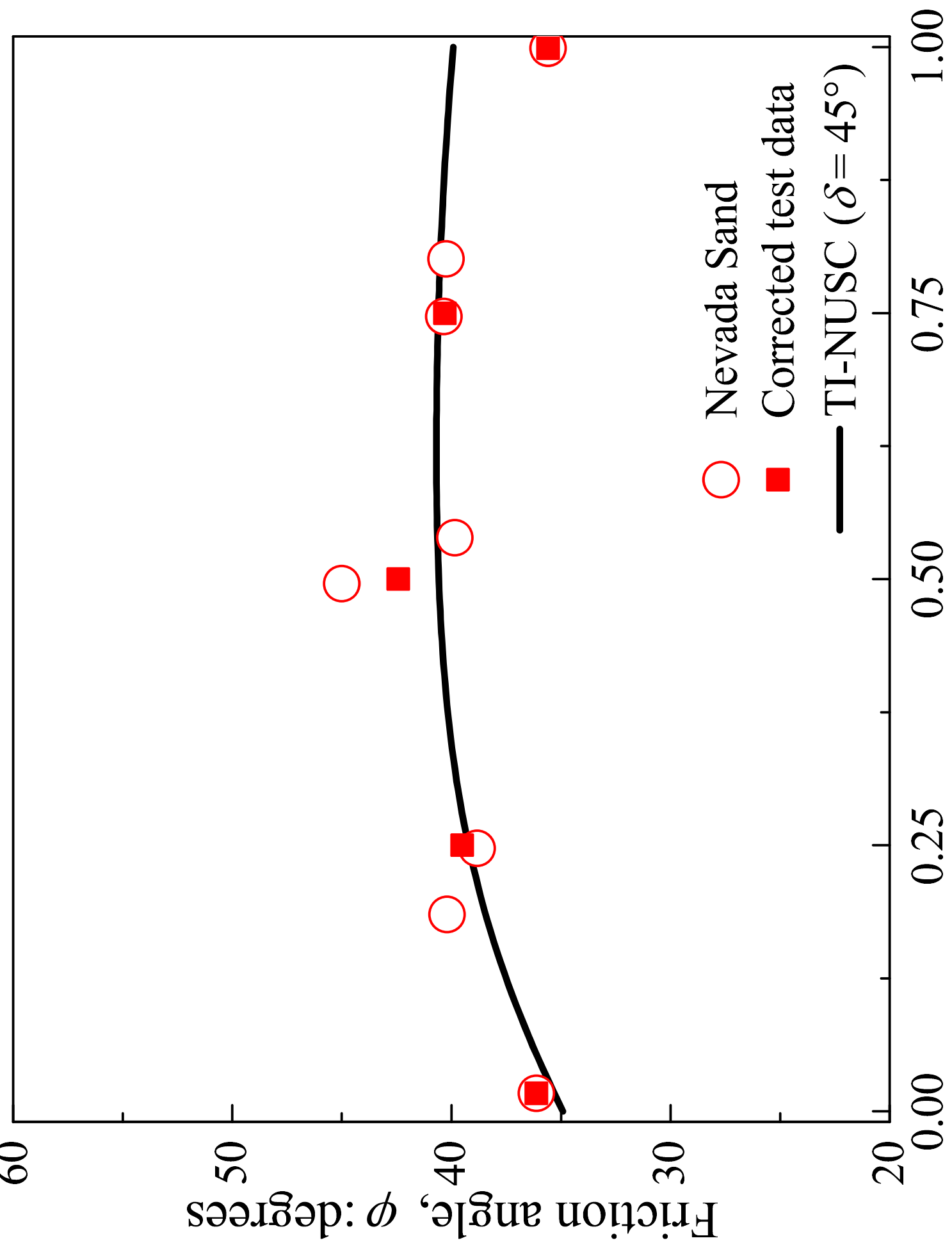




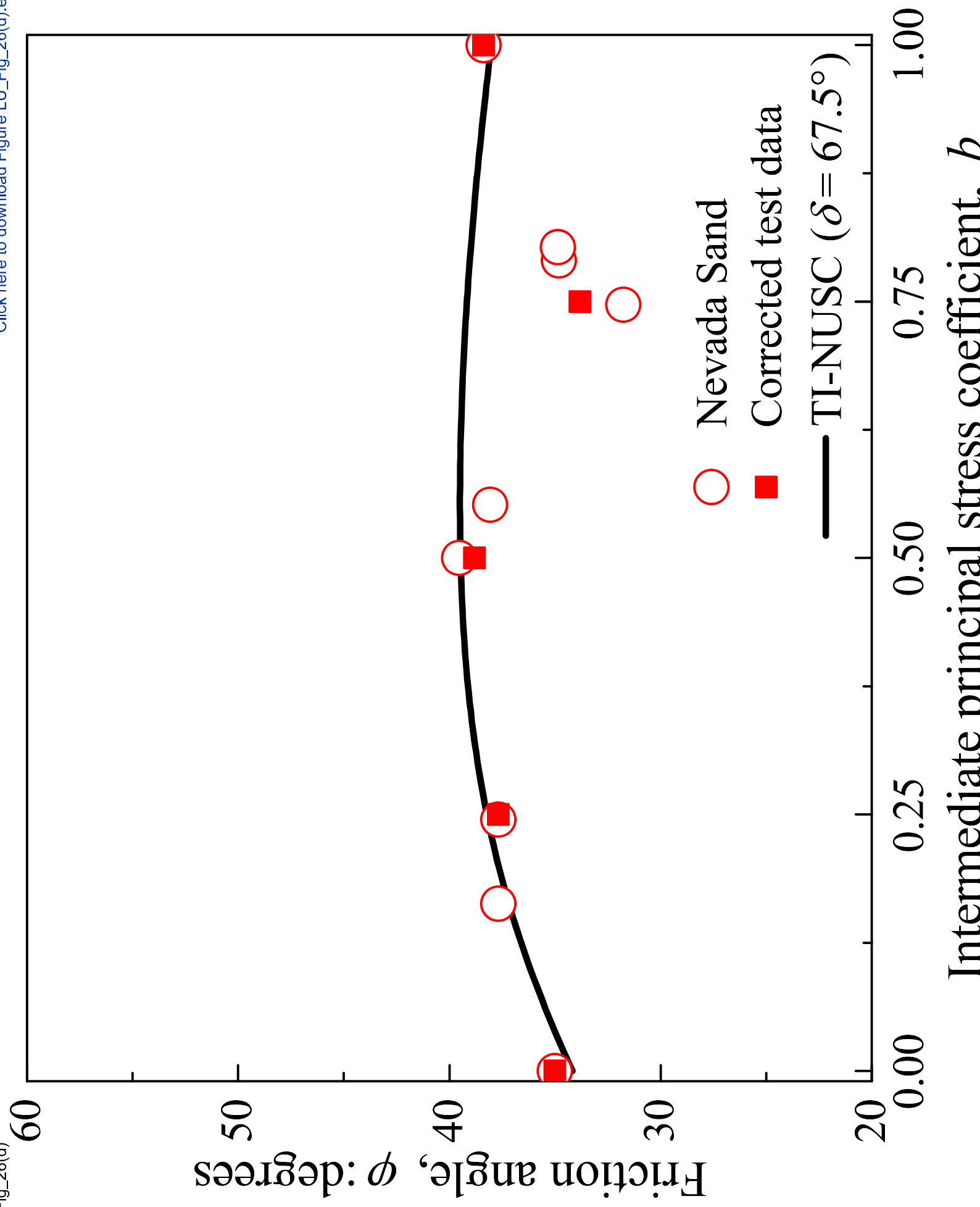
Intermediate principal stress coefficient, b

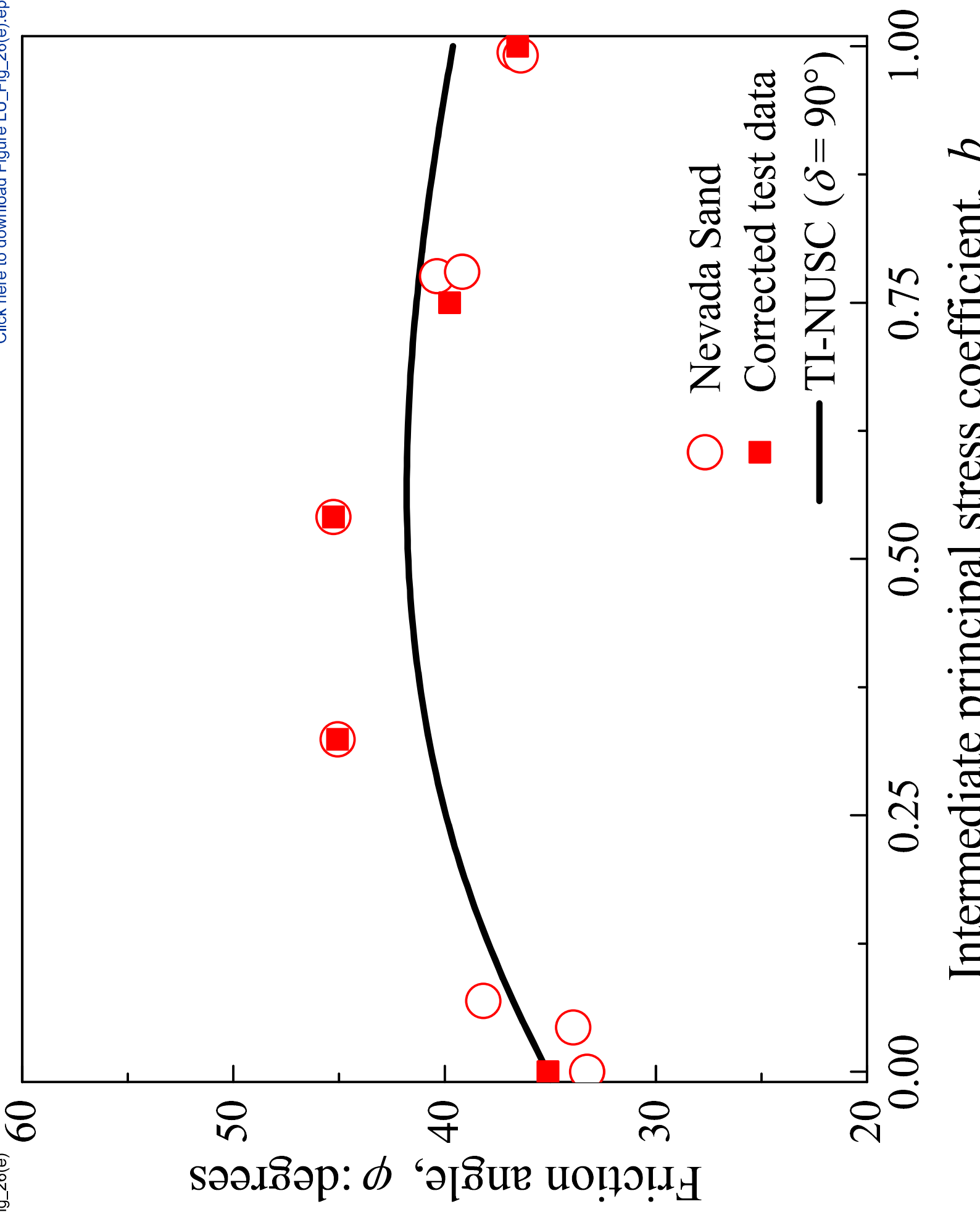


Intermediate principal stress coefficient, b



Intermediate principal stress coefficient, b





Intermediate principal stress coefficient, b

